Geophys. J. Int. (1990) **100**, 39–58

Asthenospheric viscosity and stress diffusion: a mechanism to explain correlated earthquakes and surface deformations in NE Japan

P. A. Rydelek* and I. S. Sacks

Department of Terrestrial Magnetism, Carnegie Institution of Washington, 5241 Broad Branch Road, Washington, DC 20015, USA

Accepted 1989 July 5. Received 1989 July 5; in original form 1988 July 20.

SUMMARY

A significant correlation is found, in both space and time, between the intraplate (land) and interplate (sea, thrust zone only) earthquakes in Tohoku, NE Japan that has persisted since the times of reliably reported events in AD 1600. The correlation peaks at a land-lead of about 36 yr with an average correlation distance of 200 km, with the implication of an average strain migration rate of 5.6 km yr^{-1}. The correlation is highly significant (>99 per cent), both from formal statistics and from tests of random shuffles of the data. Additional analysis of the data, as a point process, confirms the results of the correlation analysis. The sharpness of the correlation peak, when compared to the individual times of occurrence of the land and sea events suggests a trigger mechanism.

To explain the correlation, the general model of subduction–rupture–rebound is extended to include additional features; the buckling of the land plate from the force of the subducting slab, and the viscoelastic coupling of the plate to the underlying asthenosphere. A buckle produces a high-stress region in the continental plate where earthquakes are more prone to occur, thus producing the spatial correlation in the data. This may also explain the preferred location on land for the smaller modern-day seismic events in NE Japan. The viscoelastic coupling controls the interaction between the land and sea events, resulting in the temporal correlation in the data. Because of viscosity, the model equations are diffuse-like with strain pulses as solutions; thus from the inferred strain migration rate it is possible to estimate asthenospheric viscosity ($\eta = 7 \times 10^{18}$ Pa s) using this model. A large land shock generates a strain pulse that affects the locked fault at the thrust zone several decades later. As the continental plate tends to pull away from the subducting slab, the frictional force arising from the overburden pressure is reduced, thus unlocking the fault and triggering a sea earthquake.

The viscoelastic model is also used to explain surface deformations measured by triangulation surveys in Japan in 1904 and 1964. Horizontal displacements, which we believe are surface manifestations of the strain pulse from the large 1896 Riku-U land shock ($M = 7.5$) in NE Japan, are fit well by the model and provide a viscosity estimate $\eta = 13 \times 10^{18}$ Pa s.

Key words: asthenospheric viscosity, correlated earthquakes, strain deformations, stress diffusion, triggered earthquakes.

INTRODUCTION

The large-scale features of the Earth's crust that reveal the global nature of plate tectonics are subduction zones and spreading centres; both regions have been the focus of intense study in the branch of earth sciences in the past two decades. The islands of Japan are located at the subduction zones of both the Pacific sea plate in the northeast and the Philippine sea plate in the southwest (Fig. 1). Destructive earthquakes and tsunamis in and around Japan caused by the movements of these plates have been documented in historic records dating back to the seventh century AD, thus providing one of the few known earthquake catalogues (including China, Korea, Italy and South America) where

*Present address: Schiltach Observatory, Heubach 206, 7620 Wolfach, FRG.

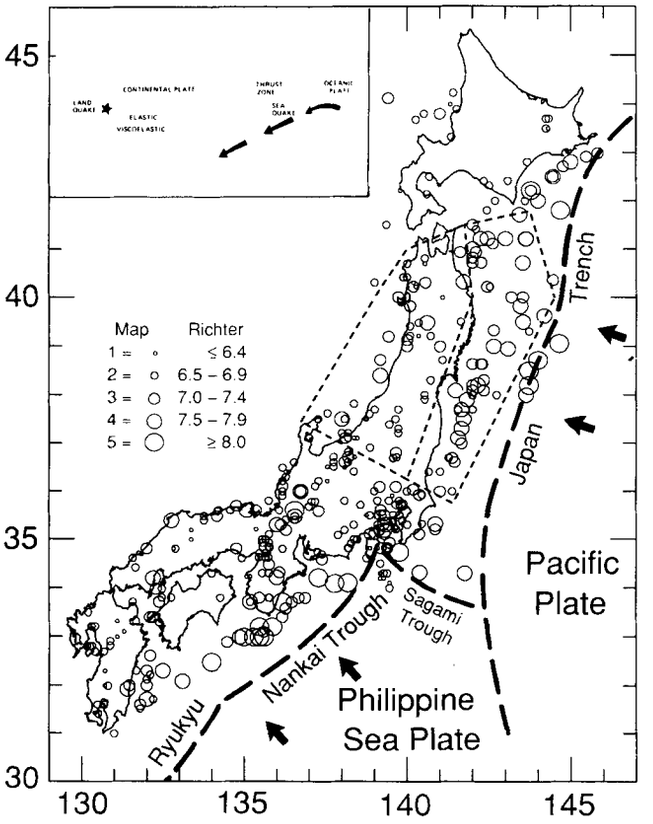

Figure 1. Map of Japan showing the magnitudes and locations of large historic and modern earthquakes compiled by the JMA. Earthquake magnitudes are scaled from 1 to 5 by the size of the circles locating the earthquakes; conversions to Richter magnitudes are given in the legend. The dashed boxes in Tohoku, NE Japan separate the land (intraplate) quakes from the sea (interplate, thrust zone only) quakes used in this study.

long-term phenomena of subduction-induced seismicity can be investigated. Modern instrument-base catalogues are limited to relatively short time spans of less than 100 yr.

In addition to their importance in the field of earthquake prediction, periodicities in seismicity provide information about the movements of the crustal plates. A study by Rikitake (1976) of large ($M \geq 7.9$) Japanese sea quakes located in the subduction zone of the Philippine plate, the Nankai Trough, showed a quasi-periodicity in recurrence times ranging from 100 to 124 yr, dependent on the location in the trough. Also, Utsu (1974) has found an 85 yr recurrence time of large earthquakes in the Kurile Trench, which is the subduction zone of the Pacific plate just northeast of the Japan Trench. These observations, however, have low time resolution, especially from a predictive point of view, as the variances of the estimated recurrence times are of the order 25–35 yr. In contrast to the above observations, no significant periodicity in recurrence time has been found in the seismicity of the Japan Trench running parallel to the eastern coast of northern Japan (Rikitake 1982).

Plate tectonic theory explains the general mechanism of thrust events in subduction zones and the quasi-periodic nature of certain types of earthquakes mentioned above. Oceanward of the subduction zone where the plate starts to bend downward, the old (>100 Myr for the Pacific plate) brittle sea plate cracks from tensional stresses and forms normal faults. In the subduction zone where it thrusts downward with constant velocity, it compresses and drags along the adjacent land plate. After the stress in the subduction zone exceeds some critical value, interplate (or sea) earthquakes are likely to occur in the form of thrust faulting between the plates, resulting in the release of the accumulated strain energy and initializing the system for the next cycle of the subduction–rupture–rebound process. Studies of seismic focal mechanisms, however, indicate that large amounts (75 per cent in the Japan Trench) of aseismic release of strain, such as ductile creep, must also be included in the above scenario to account for the long-term average slip of the plates past each other (Kanamori 1977).

No such simple model has been proposed for intraplate (or land) earthquakes. The land seismicity in Japan consists of shallow events (<25 to ~30 km) with fault-plane solutions consistent with horizontal compressional stresses in the direction of plate motion, at least where the geometry is simple as in NE Japan (Yoshii 1979). Utsu (1974) has noticed that an overall increase in land seismicity in Japan sometimes precedes large land earthquakes.

In this study of the Japanese catalogue, a significant correlation is found between the land (intraplate) quakes in NE Japan and the sea (interplate) quakes in the subduction zone of the Japan Trench; land quakes precede the sea quakes by about 36 yr. The correlation strongly suggests that the land and sea events are somehow coupled and are not occurring independently of each other, i.e. the land quakes seem to trigger the sea quakes.

To explain the correlation, we extend the subduction–rupture–rebound model to include; (a) the buckling of the land plate (lithosphere) caused by the tectonic compression of the subducting slab, and (b) the viscoelastic coupling of the land plate to the underlying asthenosphere. The extended model is consistent with the observed correlation as well as the lack of periodicity in recurrence times of earthquakes, and is in general agreement with other observations on land, such as patterns in seismicity, and surface deformations. From the correlation time and the mean distance between the land–sea events we infer a rate of strain migration which, when used in the viscoelastic model, allows us to estimate the viscosity $\eta = 7 \times 10^{18}$ Pa s (1 Pa s = 10 poise) of the asthenosphere in NE Japan.

In addition, the model is used to fit horizontal surface deformations measured by triangulation surveys after a large land earthquake (1896 Riku-U) in NE Japan. Using these data in the viscoelastic model, we obtain another independent estimate of asthenospheric viscosity of 13×10^{18} Pa s.

DESCRIPTION OF THE CATALOGUE

The earthquake catalogue used in this study was obtained by digitization of a map from the Japanese Meteorological Agency (JMA) on which the times, magnitudes, and epicentral locations of earthquakes ($M \geq 6.4$) reported from AD 671–1971 were plotted. The locations and magnitudes are shown in Fig. 1.

Some historical notes

The catalogue is not homogeneous, either spatially or temporally, but consists of three parts. Before the unification of Japan in 1600, relatively few events were recorded in the NE section. The various feudal lords were quite independent and preservations of any earthquake reports during this time should be considered to be adventitious. In the vicinity of the court in Kyoto, and some other well-established areas of the southwest, comprehensive earthquake reports during this time have survived. After the ascendancy of the Tokugawa shogunate in Edo (now Tokyo) in 1600, a well organized bureaucracy controlled all of Japan and the catalogue is more or less uniform. The reporting of small events is, of course, dependent of the population density as is the intensity assessment.

The shogunate collapsed in 1868 and after a short period of confusion, as far as reporting of earthquakes is concerned, the modern catalogue commenced. Professor John Milne was appointed to the Imperial University in 1875 and founded the Japan Seismological Society in 1880; after 1890 the number of reported events increases substantially (Fig. 2). Inspection of Fig. 2 suggests that the magnitude of the events before 1890 could be underestimated by up to a magnitude unit relative to the modern events. We assume that there has been no change in the seismicity, and therefore that the apparently greater rate of large earthquakes after 1890 is an artifact. Another difference is noticed in the record of the sea quakes. In the earlier portion of the catalogue, the larger sea events that produced damaging tsunamis along the coast were certainly reported, although smaller shocks may have been missed; these types of events were reliably and more frequently located after 1890. Thus we assume that after 1600 our catalogue is complete only with regard to the larger events.

Selection of Earthquakes

In this study, the boxed section in NE Japan in Fig. 1 is chosen because this portion of the Pacific subduction zone has several unique features: (1) the strike of the subduction zone is mostly linear, (2) the zone is well isolated from the edges of adjacent subduction zones; the box excludes the Philippine sea plate in the south and the sweeping bend of the subduction zone between the Japan and Kurile Trenches in the north, (3) statistically, there is a reasonably adequate sampling of historic seismicity both on land and in the sea, and (4), most importantly, the motion of the subducting slab, inferred from studies of deep and intermediate focus earthquakes, fits the simplified model of subduction. In this region, the old (>100 Myr) oceanic plate subducts at approximately normal incidence to the Japan coast and once past the thrust zone, the slab sinks with minimal contortion at about 30° dip to great depths (Yoshii 1979).

The boxed section in Fig. 1 is divided to separate the land quakes from the sea quakes (see Table 1). Several events along the inner boundary of the box could be changed from land to sea (and vice versa) by slightly redrawing the boundary, but for the most part our division correctly separates the two types of earthquakes. Also, several large earthquakes near the axis of the Japan Trench are omitted since these are presumably large normal-faulting shocks caused by the initial bend of the sea plate as it starts to subduct and are not considered in the subduction–rupture–rebound model. We point out that the boxed section is the

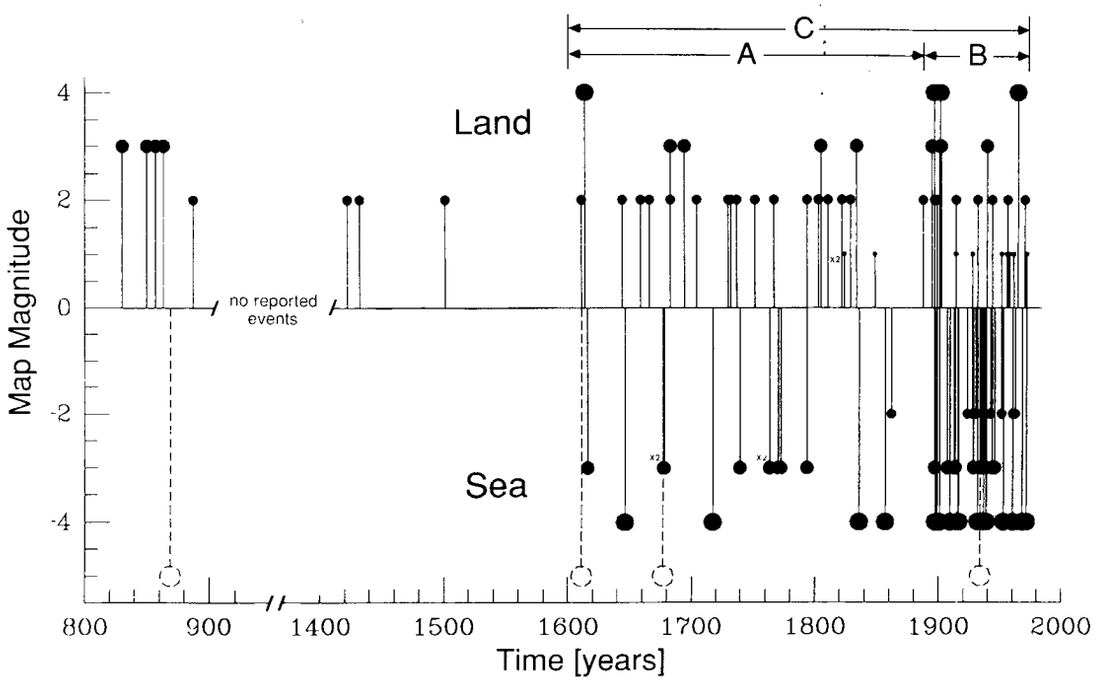

Figure 2. Record of land and sea quakes from the boxed sections of Fig. 1. Circles and solid vertical lines are scaled to map magnitudes and the dashed entries mark large earthquakes seaward of our boxed region. Sea events are drawn inverted, and with negative magnitudes for clarity. Windows A and B divide the catalogue into independent records with different but mostly stationary rates of earthquake occurrence. Window C is A + B. Notice that there were no *reported* earthquakes in this region of Japan from AD 900 to 1400.

Table 1. Listing of events.

LAND				SEA			
Year	Latitude	Longitude	Map* Magnitude	Year	Latitude	Longitude	Map Magnitude
1611	37.5	139.6	2	1616	38.1	142.0	3
1614	37.5	138.0	4	1646	37.7	141.7	4
1644	39.4	140.1	2	1677	36.6	141.5	3
1659	37.2	139.7	2	1678	38.6	142.3	3
1666	37.1	138.2	2	1717	39.0	142.6	4
1683	36.7	139.6	2	1739	40.7	142.3	3
1683	36.8	139.7	3	1763	40.7	142.0	3
1694	40.2	140.2	3	1763	40.8	142.0	3
1704	40.4	140.0	2	1770	38.6	142.0	3
1729	37.6	137.6	2	1772	39.3	142.6	3
1731	37.9	140.5	2	1793	38.3	142.4	3
1736	38.3	140.7	2	1835	37.9	141.8	4
1751	37.2	138.0	2	1856	41.2	142.2	4
1766	40.8	140.5	2	1861	37.7	141.6	2
1793	40.7	140.0	2	1896	36.0	141.0	3
1802	37.8	138.4	2	1897	38.1	141.5	4
1804	39.0	140.0	3	1898	39.5	143.5	4
1810	39.9	139.8	2	1900	41.0	142.0	4
1821	37.4	139.5	2	1907	40.2	142.5	3
1823	40.0	141.1	1	1909	41.2	143.0	3
1828	37.6	138.8	2	1912	38.6	142.3	3
1833	38.7	139.2	3	1913	41.5	142.0	3
1848	40.7	140.5	1	1915	38.9	143.1	4
1887	37.7	139.0	2	1916	41.2	143.6	3
1894	39.2	139.4	3	1923	36.0	141.4	2
1896	37.5	137.3	2	1927	38.0	142.0	2
1896	39.5	140.6	4	1928	40.0	143.2	3
1898	36.9	138.9	2	1930	36.4	140.7	2
1900	39.0	141.0	3	1931	41.2	142.5	4
1901	40.3	141.7	4	1933	38.1	142.4	3
1902	40.9	141.6	3	1935	36.7	141.3	2
1914	39.2	140.4	1	1935	40.0	143.5	3
1914	39.5	140.4	2	1936	38.2	142.2	4
1927	37.5	138.8	1	1937	38.2	142.0	3
1931	39.5	141.6	2	1938	36.4	141.0	2
1939	40.0	139.7	3	1938	36.7	141.4	3
1943	37.3	139.7	2	1938	37.0	141.7	3
1951	37.1	138.5	1	1938	37.1	141.6	4
1955	40.3	140.2	1	1938	37.3	141.7	4
1956	38.0	140.5	2	1938	37.5	141.7	4
1957	40.2	140.3	1	1942	37.7	142.0	2
1961	37.5	138.7	1	1943	41.1	142.6	3
1962	38.7	141.1	2	1945	40.9	142.1	3
1964	38.4	139.2	4	1951	41.4	142.1	2
1970	39.2	140.7	2	1952	41.7	143.4	3
1971	37.1	138.4	1	1960	39.8	143.5	4
				1960	40.2	142.5	2
				1962	38.0	142.7	2
				1968	40.7	143.5	4
				1971	41.2	143.6	3

* Conversion to Richter magnitude in Fig. 1 legend.

first and only division that was used, i.e. the box was not relocated by trial-and-error to optimize the results presented below.

A plot of the time history of the land and sea quakes in the boxed section of the map is shown in Fig. 2. (Earthquake magnitudes are scaled 1–5 by the circle size in the original JMA map; conversions to Richter magnitudes are listed in the legend of Fig. 1.) Notice the large increase in the number of reported earthquakes after 1890 due to the establishment of the Imperial Meteorological Agency (now the JMA) and the advent of seismic instrumentation. Because of this demarcation in the catalogue and because the sea record contains no reported earthquakes before 1600, three time windows are formed; window A is from 1600 to 1890 with 24 land and 14 sea events, window B is from 1890 to 1971 with 22 land and 36 sea events, and window C is the sum of A plus B; thus windows A and B form independent catalogues.

METHODS OF DATA ANALYSIS

In this section, we show that the land and sea events in the above windows are correlated. Because of the important conclusions drawn from the correlation, it was thought advisable to use two independent methods of analysis. In the first, the data is treated as a continuous process by the methods of time series analysis and in the second as a point process using the statistics of random variables.

Continuous process; correlation function

The difficulty in transforming a point process, such as our earthquake record, into a pseudo-continuous process is discussed in detail by French & Holden (1971). As we are interested in large-scale features and long-term phenomena of tectonic origin, an adaptation of their work is used to form a continuous variable of earthquake data as follows. All earthquakes occurring within an assigned time interval τ are treated as a single weighted event. This is achieved by first filling the record between earthquakes with zeros to form a continuous time series of yearly samples in which the earthquake magnitudes form a set of delta functions in time. This time series is then digitally filtered by the application of a single-pole high-pass filter with a cut-off of τ yr. Thus earthquakes occurring within τ yr appear as lengthy integrated events, while earthquakes or clusters of

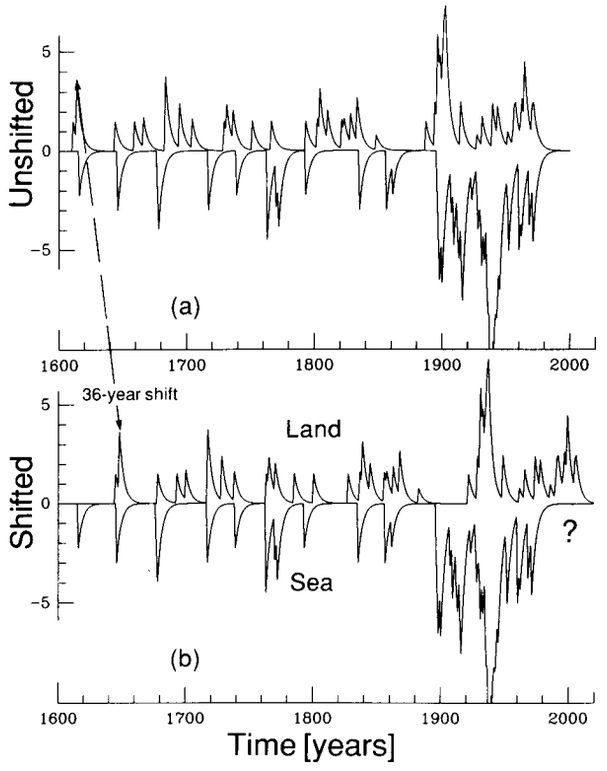

Figure 3. High-pass filtered records from windows A and B of Fig. 2 for (a) the original data and (b) the land record, time shifted by 36 yr. The ordinate is map magnitude as in Fig. 2. The sea record is drawn inverted for clarity.

earthquakes separated by more than τ yr tend to appear isolated in time. (Here the distance between events is neglected but this point will be covered later.) The results described below are obtained using $\tau = 3$ yr because this cut-off seems to group together most of the obvious clusters of events. The filtered earthquake records, shown in Fig. 3(a), are then analysed by standard methods of correlating two continuous processes (e.g. Bevington 1969). The overall value of the correlation function at any lag will, of course, depend on τ. A very small τ will produce pulses looking like the original comb of delta functions and the correlation will be small since events are likely to miss each other; a very large τ will force larger correlations since this spreads out the earthquakes in time and overlapping coincidences will occur more often. Thus extreme values of τ will significantly affect our results. However, our choice of τ was varied by 50 per cent and the results were found to be stable. The results were also found to be insensitive to the actual type of high-pass filter used.

The autocorrelations (not shown) of the land quakes, the sea quakes, and the sum of land and sea quakes show no significant structure in any of the three windows, which supports the previously mentioned claim of Rikitake (1982) of non-periodicity in the recurrence times of earthquakes in this part of northern Japan. (It also agrees with our findings in the next section that the sequences of land and sea events are individually randomly distributed.)

The cross-correlations (Fig. 4) of the land versus the sea quakes, however, show a significant peak (>99 per cent confidence) in all three windows when land quakes lead the sea quakes by 34–38 yr. There is also a significant correlation peak in window B when land lags sea by about 28 yr. Formally, both correlations (36-yr land-lead and 28-yr land-lag) are found in the modern catalogue in window B. Closer inspection of the record in this window shows that these correlations are caused by bursts of land activity near the ends of the window correlating with the sea burst near the centre. Thus both of the correlation peaks are biased by single bursts of activity and should be viewed with caution. However, the important point in Fig. 4 is that the land-lead correlation peak is highly significant in both independent

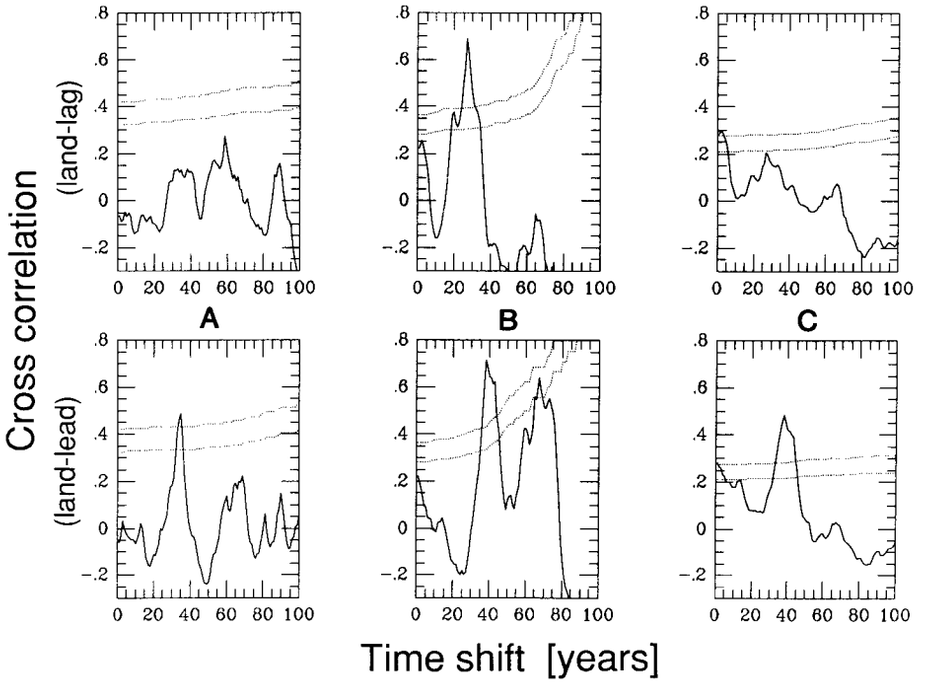

Figure 4. Cross-correlations of the land versus sea records as a function of land-lag/lead for windows A, B, and C. Upper and lower dotted lines are 99 and 95 per cent confidence levels, respectively.

windows A and B, and in the combined window C. This is the only peak which is phase coherent across the entire catalogue; other peaks are not persistent throughout the windows and are cancelled by the addition of more data. Confidence levels in the correlation plots are drawn from the formal statistics of the linear correlation coefficient of n degrees of freedom; in this case n is set equal to the number of events in the overlap between the land and sea records being correlated (Bevington 1969). Even though window B is shorter than window A, it has a higher rate of earthquake occurrence, which explains why the confidence levels in Fig. 4 for windows A and B are similar, at about 36 yr.

Different aspects of the earthquake record were also correlated, such as: earthquake energy instead of magnitude using a standard energy–magnitude relation, downgrading a few of the larger land and/or sea shocks to smaller magnitudes, and assigning a constant magnitude to all shocks. The cross-correlations of all our altered data sets showed the 36-yr pear to be persistent.

To display the land–sea correlation, the earthquake records with the land events time-shifted forward by 36 yr have been replotted in Fig. 3(b). As noted above, window B alone is too short to provide a convincing correlation, but window A, and its forward extension to window C, clearly reveals a correlation between the land and sea events.

Bootstrap analysis by random shuffles

In order to assess the significance of the correlation coefficient of 0.49 obtained from the data, the probability that such a correlation can be obtained by chance was investigated. The land events in window A only (considering again the shortness of window B) were randomly shuffled by assigning the earthquakes new origin times from a uniform random distribution spanning the length of the window. This shuffling procedure is a variation of the bootstrap method of computer-intensive data analysis (Diaconis & Efron 1983). Both the value of the maximum cross-correlation and the corresponding lag were tabulated for 10 000 trials of random shuffles and the tabulations plotted as histograms, shown in Fig. 5. If the observed 36-yr correlation peak was an artifact, produced by the location of the largest sea events, then a similar artifact would be seen in the histogram from the random shuffles. Nothing anomalous is apparent at 36 yrs (or other lags) in Fig. 5(b), only a steady rise in the histogram with longer ± lags, which is explained by the expected loss in the total events caused by the lagging process. Equally important is that the histogram of the maximum cross-correlation peaks at about 0.30 compared to the observed maximum of 0.49, and the spread is such that only 0.4 per cent of the random shuffles exceeds the observed value; it is difficult to obtain a correlation as good as the real observed correlation by a random shuffle.

Point process statistics

In this section, the earthquakes are considered as a point process and the procedure outlined and used by Kagan & Knopoff (1976) in their search for non-random features of the seismicity of strong earthquakes is followed. Kagan & Knopoff studied the second-order moment of their catalogue, which is a form of conditional probability, calculated by finding the number of earthquakes in a certain space–time–magnitude interval from any given shock. A random (i.e. uncorrelated) catalogue would show no statistically significant pairing of events.

From a significance test, which compares the cumulative number of shocks in time against a Poisson process (see e.g. Cox & Lewis 1966), the individual land and sea records in our windows are found to be Poissonian in character and thus can be characterized by a first-order moment which is the average rate of occurrence of events. There are, of course, different rates of occurrence in windows A and B for both the land and sea events. Since the sum of two Poisson variables is another Poisson variable, higher moments of the process other than first-order need to be studied to reveal a correlation between the land and sea events (Kagan & Knopoff 1976; Reasenberg 1985.). To avoid the complications of computing the higher-order statistics of a Poisson process having a non-stationary rate, as in window C, we focus on window A alone; this window is the longest and showed the clearest correlation from our analysis in the previous section.

The second-moment of window A is calculated by finding all pairs of land–sea events in a given time–distance interval from the land shock of the pair. No magnitude limits were used because of the paucity of events in window A and also due to awareness of the probable sources of error in estimating the magnitudes of the historic shocks. As a first step, the point process analogue of the correlation function

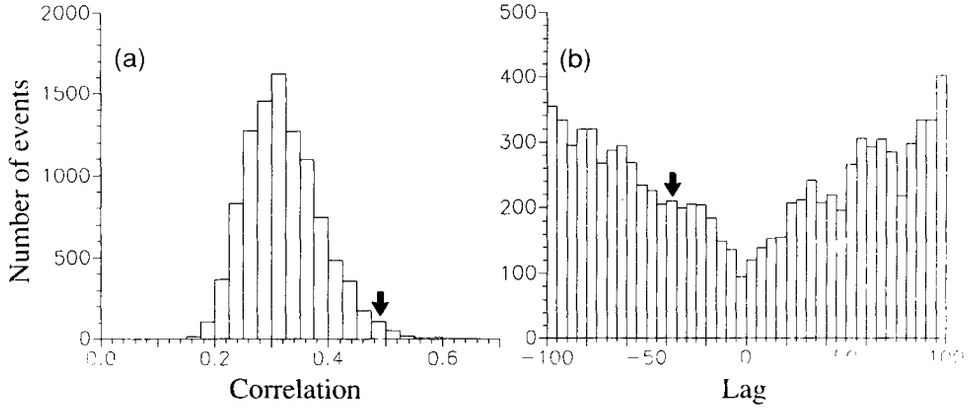

Figure 5. Histograms of (a) the maximum value of the cross-correlation and (b) the lag at which it occurred for 10 000 random shuffles of the land events in window A only. Arrows mark the values of the observed correlation peak in Fig. 4 for window A.

is calculated by finding the total number of land–sea pairs, within the time interval t and $t + \Delta t$, where t spanned ± 100 yr with $\Delta t = 4$ yr. In this step we omit the distance between events but this is included in the next step. The total number of land–sea pairs per interval Δt is shown in Fig. 6. Having found that the individual land and sea earthquake occurrence is Poissonian, the rate of occurrence of all pairs of shocks may be calculated from the combined set of the land and sea records in window A, i.e. the sum of two Poissonian processes. This Poissonian rate (ν_P) is calculated by simply adding up all pairs of shocks, using any combination of land–land, land–sea, or sea–sea events, that occurred in the wihdow and then by dividing by the length of the window; this forms an unbiased estimate of the rate of pair occurrence for a Poisson process, which is the case for our combined land and sea records. Using ν_P we calculate (at a given probability level) the expected number of earthquake pairs in Δt and compare this number to the actual values in Fig. 6. It is found that the observed number of land–sea pairs in the time interval $-38 < t < -34$ yr, has a less than 1 per cent probability of happening by chance in a Poisson process with rate ν_P.

A simple way of viewing the foregoing analysis is as follows. All the land and sea events are mixed and then pairs are selected at random. If events are uncorrelated, then pairs selected from all window A shocks (land + sea) should have the same probability whether it is a land–land, land–sea, or sea–sea pair. If there exists a significant land–sea correlation, then these pairs will be selected more often than other pairs, assuming a fixed time interval between shocks for any run of selections.

In this step, distance between events is included in the analysis by spanning the distance interval ΔR, from 50 to 450 km in 100 km increments. This grid is not coarse when the magnitude of the earthquakes used and the possible location errors in the data from this older portion of the catalogue are considered. The 50 km offset is chosen to allow for the initial bias in the distance between events because of the way the map has been divided. The second moment is displayed as a matrix in Table 2, where the rows and columns are the distance and time intervals,

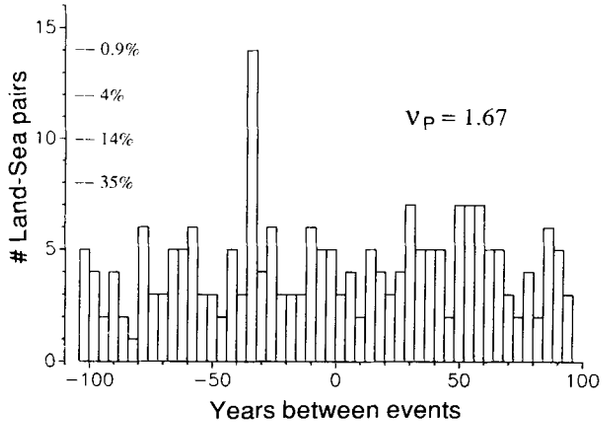

Figure 6. Plot of the number of land–sea pairs from window A in 4-yr time increments spanning ±100 years. Negative abscissae are land leads, positive are land lags. Percentage values are the probabilities, calculated from the Poissonian rate ν_P, of obtaining by chance a given number of pairs in any 4-yr increment.

Table 2. Space–time moment analysis of the land–sea records.

Distance (km)	Land-Lead Time* (years) 58	54	50	46	42	38	34	30	26	22
50–150	1	.	.	.	.	.	1	.	.	.
150–250	3	.	.	1	1	2	6	1	1	.
250–350	2	.	2	1	1	1	2	3	4	1
350–450	.	.	1	.	2	.	2	.	.	1

* The centre time of a 4-yr bin.

respectively, and the matrix elements are the total number of pairs of land–sea events in any given time–distance interval. As in Fig. 6, for any row in the table, the probabilities of obtaining the observed entries compared to the expected values from a Poisson process, i.e. the combined land and sea records, are found. These are given in Table 3 for each row. Table 3 includes a correction factor to account for the geometrical constraint imposed by the shape of the location boxes in Fig. 1. The correction factor was determined by filling both land and sea boxes with random events distributed uniformly in space and then drawing random pairs to find the effect of increasing distance between pairs.

The largest count of six pairs, with a probability of chance occurrence of 0.5 per cent, is the matrix element corresponding to a land-lead spanning a time interval of 32–36 yr and a distance interval of 150–250 km. Although some rows in Table 2 have entries (three or four pairs) with a relatively small probability of chance occurrence (~5 per cent), inspection of the earthquake record shows that these entries are formed mainly by land–sea pairs of the smallest shocks. In comparison, the least probable entry of six pairs consists primarily of pairs of the largest shocks. This is also seen in Fig. 3(b) and is consistent with our earlier observation that earthquake energies produced a good correlation peak at 36 yr. In general, the spatial correlation is not as peaked as the temporal correlation but this is not unexpected since the origin times of the earthquakes are known precisely (in terms of the year of occurrence) compared to the estimates of epicentral locations.

Additional evidence from old events

An observation which lends support to our claim of a land–sea correlation can be found in the oldest portion of the catalogue. As noted earlier, a group of large magnitude ($M > 8$) events in Fig. 1 just seaward of the thrust zone are

Table 3. Poissonian probabilities for entries in Table 2.

Number of Pairs	Distance (km) 50–150	150–250	250–350	350–450
6	0.13%	0.50%	0.21%	0.02%
5	0.70	2.03	1.00	0.17
4	3.14	7.02	4.11	1.07
3	11.45	20.02	13.83	5.33
2	32.72	45.42	36.61	20.57
1	>50	>50	>50	>50
$\nu_P \Delta t$	1.172	1.536	1.280	0.840

excluded from our analysis as they are taken to be normal-faulting shocks not considered in the subduction model. In the modern catalogue, these types of events are well located but in the older catalogue they could conceivably be mislocated thrust zone events. Including these events in the analysis of the non-modern catalogue adds two sea quakes in window A (1611 and 1677 in Fig. 2) but these occur at or near times of other sea quakes and cause no significant changes in our correlations and conclusions. In the oldest portion of the catalogue, however, the land activity commencing in AD 830 was followed by a large sea earthquake in AD 869, in complete agreement with the foregoing analysis (see Fig. 2). In fact, the only obvious missed correlation of the larger pulses in Fig. 3(b) is a lack of land activity around 1860 to correlate with the sea activity at about the turn of the century.

SUBDUCTION MODEL: SUBDUCTION–RUPTURE–REBOUND

Intraplate (land) and interplate (sea) earthquakes caused by the subduction process can be explained by the generally accepted elastic model of subduction–rupture–rebound shown in Fig. 7. Because there are both land and sea quakes, the slow accumulation of tectonic compression must first sweep the internal stress in the land plate past the threshold of elastic failure because the following sea quake in the thrust zone relieves the compression, thus initiating the next cycle of the process. In this cyclic model, time windows of low and high probabilities of earthquakes occurring on land are expected. The land earthquakes are more likely to occur at any time when the probability is high; therefore, the time interval between land and sea earthquakes will exhibit a broad-band distribution rather than the correlation peak observed. Nevertheless, this simple model does show why the land quakes precede the sea quakes; Shimazaki (1978) and Seno (1979) pointed this out from a study of the more recent seismicity (1850–present) in Tohoku, NE Japan.

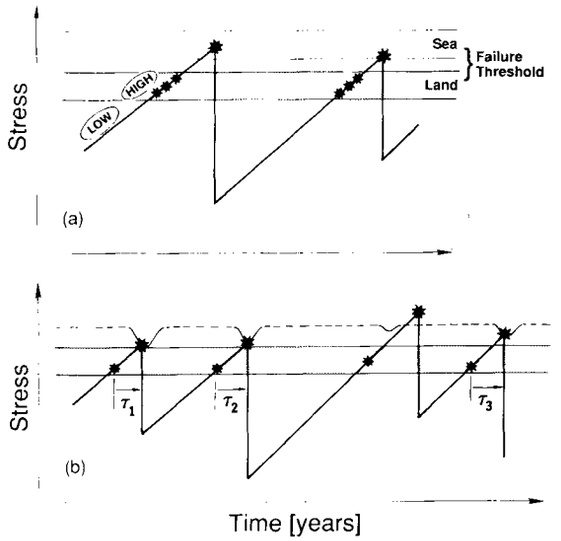

Figure 7. Models of failure in the subduction process. (a) The tectonic stress gradually increases and sweeps past the critical level for land earthquakes but is eventually reset after a large sea quake, thus forming a cyclic pattern in the earthquake recurrence cycle. Times before and after the stress curve crosses the land threshold in any cycle will correspond to times of low and high probability of seismic activity on land. (b) Here the strain pulse from the previous land quake produces a temporary lowering of the sea threshold, and sea quakes are more likely to occur when the stress buildup intersects the new threshold. The lowering is because the pulse reduces the static frictional force, thus unlocking the fault between the plates; the physical properties of rocks are unaffected. In another sense, the sea shocks are triggered because the land plate is pulled away from the sea plate by the action of the pulse (see Appendix B). Note that the times τ_i between land and sea events form a narrow grouping when compared to the time intervals between land or sea events taken individually. The penultimate sea shock in the figure is not triggered, thus failure occurs as shown in (a).

In the perfectly elastic model, each class of events is responding in an independent manner to the tectonic forces. Thus the model precludes the possibility of an interaction between events (other than pure–elastic propagation effects) and no correlation is possible between the land and sea shocks. We extend the elastic model to include the buckling of the continental plate from subduction forces and the viscoelastic coupling of the continental plate (lithosphere) to the underlying asthenosphere. The buckle results in a preferred location in the lithosphere for the land events (hence the spatial correlation), and the asthenospheric coupling provides and governs the interaction between the land–sea events (hence the temporal correlation).

Buckling of the continental lithosphere

A quantitative theory describing the response of the continental plate to the compression and torque from the subducting slab is not yet available, but we speculate that the continental plate will buckle and bulge (Fig. 8). Turcotte

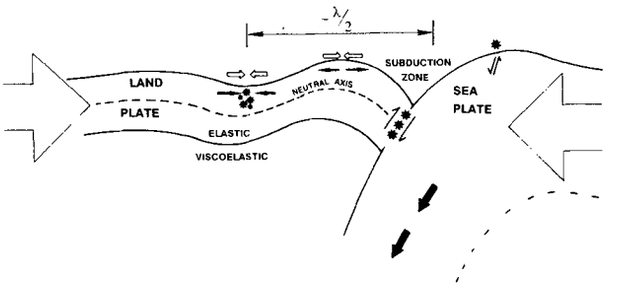

Figure 8. Sketch showing the deformed (grossly exaggerated) land and sea plates at a subduction zone. In the region studied, the subducting Pacific plate is more than 100 km thick whereas the elastic continental lithosphere of NE Japan is about 30 km thick. Bending and extension of the sea plate just seaward of the thrust zone produces large normal-faulting earthquakes. In the thrust zone, the tectonic compression and torque from the subducting slab forces the land plate to buckle. Superposition of stresses of tectonic origin (outlined arrows) with those from the buckle (horizontal solid arrows), forms a highly stressed seismically active zone ($\sim\lambda/2$) as well as a de-stressed zone within the land plate. The buckled plate is viscoelastically coupled to the underlying asthenosphere. Because of this, intraplate earthquakes produce strain pulses which diffuse outward at a rate dependent on plate thickness and asthenospheric viscosity. These pulses may trigger earthquakes in the locked thrust zone.

& Schubert (1982) have modelled the flexure on the oceanic side of the trench in subduction zones. Their model explains the upwarping of the trench oceanwards and matches the bathymetry well. We expect that similar upwarping will occur on the continental side as well. The resultant deformation (sketched in Fig. 8) results in regions of tensile and compressional stress separated by neutral unstressed zones. This internal stress is superimposed on the overall tectonic compression, resulting in further zoning of stressed and unstressed regions within the plate. Higher stresses are found where the tectonic and deformational stress reinforce each other ($\sim\lambda/2$ in Fig. 8), and lower stresses where they tend to cancel ($\sim\lambda/4$). [Sacks *et al.* (1978) used the ideal of stress cancellation to explain the existence of an aseismic wedge between the shallow earthquakes in the subducting plate and those in the continental plate in southern Peru.] Significant enhancements of elastic stress are restricted to the upper portion of the plate, because below a certain depth ($\sim$20 km) the intraplate seismicity in northern Japan is greatly reduced, implying that stress redistributions at depth occur by non-brittle mechanisms such as ductile flow. In a uniform buckled plate, earthquakes are therefore more likely to occur in higher stress regions ($\lambda/2$ in Fig. 8) and will not be scattered randomly throughout the plate. This is important because if the epicentres of land events were randomly distributed, then a narrow correlation peak should not be observed in the data. Formally, the Turcotte & Schubert (1982) model does not produce a buckle since the shape of the deformed plate is that of a critically damped sinusoid. However, the addition of the long term horizontal compression might produce a buckle, though it is unclear how the 'wavelength' of the buckle will be affected by the additional stress. Certainly it will be decreased. Rigorous evaluation of deformation resulting from the downward drag of the subducting plate as well as the horizontal compression of a continent with variable geology, lithosphere thickness and faulting systems, will be a formidable task. Note that the buckling hypothesis is not essential to explain the land–sea correlation; any mechanism which concentrates seismicity, such as geological features or non-uniform plate thickness, is the only requirement.

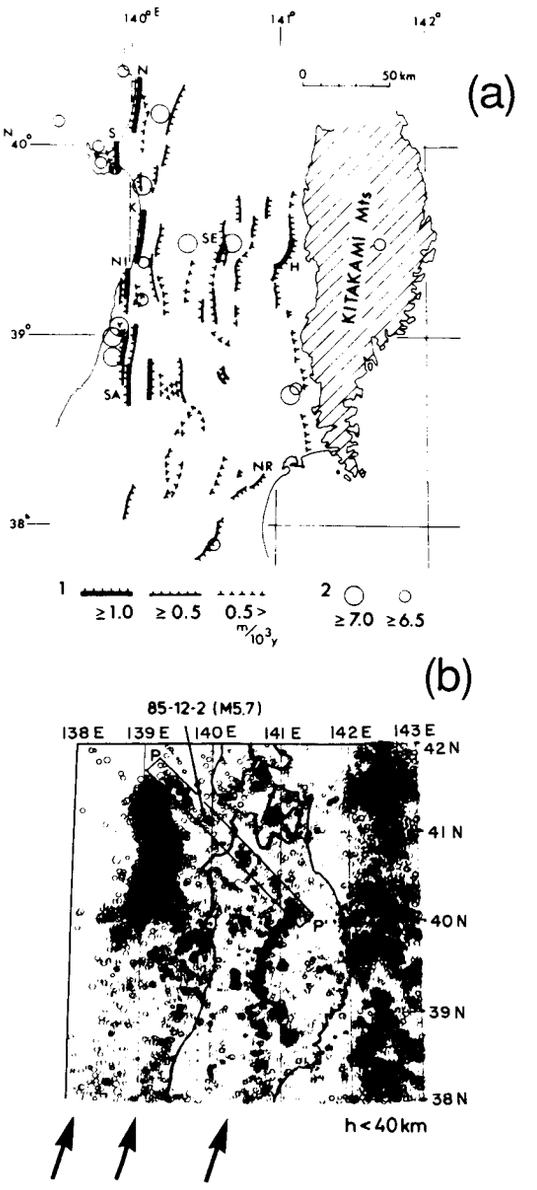

Figure 9. (a) Distribution of major Quaternary faults and larger earthquakes in Tohoku, NE Japan; ticks are drawn on the upthrown side of the fault (from Awata & Kakimi 1985). (b) Plot of shallow seismicity ($\leq$40 km), circles indicate earthquakes, from 1981 January to 1986 January. The broad swath of seismicity on the right shows the interplate thrust events. The right-hand arrow shows a concentration of seismicity striking slightly east of north which may be due to the buckle. The central arrow indicates the earthquake concentration off the west coast. This could be due to a buckle but there is also a structural discontinuity there. The cloud off the NW shore is an aftershock sequence.

Seismic evidence of a buckled plate

The historical seismicity in NE Japan suggests that there are preferred locations for earthquakes on land. The large land earthquakes ($M \geq 7.5$) in this region are associated with the movements of fault blocks (Awata & Kakimi 1985). The blocks create a network of faults which run parallel to the major trend of the island arc (Fig. 9a), thus resembling a pattern not unlike that formed by the higher stress region in a buckled plate.

The smaller present-day earthquakes also reveal a pattern of concentrated seismicity. If these events are occurring in the higher stress regions on land, then they should illuminate this portion of the buckle; there are, of course, other localized sources of stress which cause earthquakes. Indeed, this pattern can be seen in bands of active shallow seismicity ($\leq$40 km) in Tohoku, NE Japan (Fig. 9b). From the figure we estimate $\lambda \sim 150$ km which is identified with the high stress region in Fig. 8.

Viscoelastic coupling of the lithosphere to the asthenosphere

The introduction of viscosity into the model provides an interaction between the land and sea events. A large intraplate earthquake will fracture the lithosphere to relieve the stress and relax the plate. This relaxation is unlike the response of the pure-elastic model because the bottom of the lithosphere is viscoelastically coupled to the asthenosphere. The solution to the problem of an edge dislocation

(thrust earthquake) in an elastic plate (lithosphere) over a viscoelastic channel (asthenoshere) is given in Appendix A. This model was originally developed by Heinze & Sacks (1979) to explain post-seismic strain changes measured by geodetic networks in northern Japan. Because we model actual faults in the lithosphere as 2-D (line) sources, the range of applicability for the larger shocks ($M \geq 7.3$) is for distances of ~50 km from the fault centre out to at least 2–3 × source dimensions. Geometric spreading effects for finite-length faults will result in an over-estimate of the strain at larger distances but the model adequately spans the mean distance of the land–sea correlation found in this study. Post-seismic strains from smaller shocks, analogous to point sources rather than line sources, would drop off much faster with distance than a simple downward scaling of the larger shocks.

The solutions to the equations of the viscoelastic model in Appendix A are diffuse-like strain pulses. Examples showing the time dependence of the strain field from a thrust source (1 m of displacement) are given in Fig. 10(a) for different observations distances. The times at each distance where the strain rises to $[1 - \exp(-1)] = 63$ per cent of its maximum value are also indicated. The distance divided by this time is the definition of the velocity in this model (see further discussion in Appendix A). The velocity of a pulse is a function of the two unknown model parameters: it is proportional to the effective elastic thickness H_e of the lithosphere and inversely proportional to the viscosity η of the asthenosphere. (The full description of the strain field in Appendix A is parametrized by H_e, and η, as well as rigidity μ and source slip u_0. But $\mu = 100$ GPa is determined from laboratory measurements, and our definition of velocity makes u_0 arbitrary.) Using post-seismic uplift data collected within ±40 km of the fault of a large land shock in 1896 (Riku-U in NE Japan), Thatcher *et al.* (1980) determined $H_e = 30$ km with less than a 5 km uncertainty, a value in close agreement with that obtained by the Research Group for Explosion Seismology (1977). Therefore in our model, the unconstrained parameter affecting the velocity is the viscosity. In Fig. 10(b) curves of velocity versus distance are plotted for several values of viscosity pertinent to the asthenosphere. The strong dependence of pulse speed with distance, especially at shorter distances (<~120 km), is clearly seen in the figure.

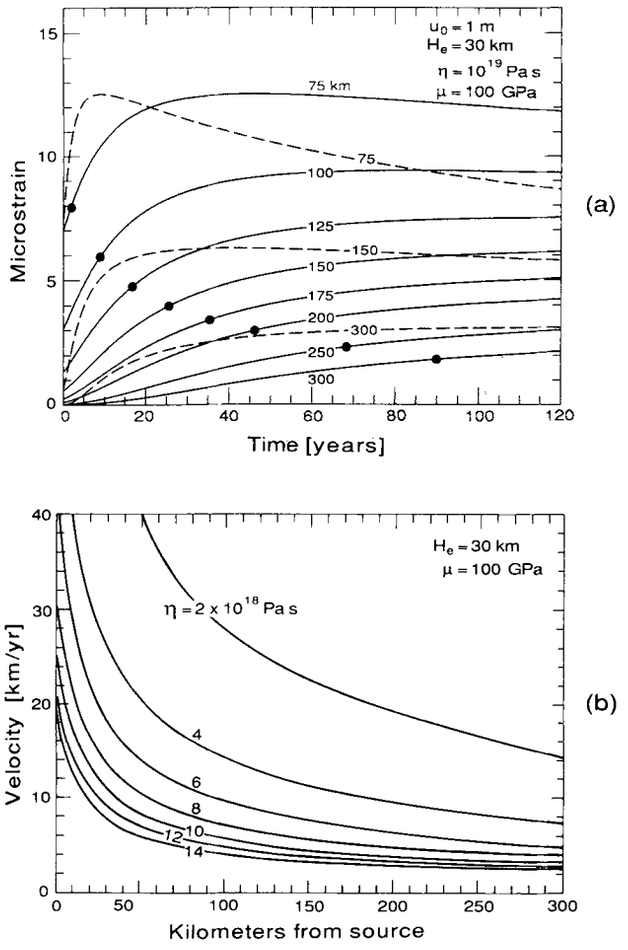

Figure 10. (a) Strain versus time plots for different distances from the source. The model parameters are given in the legend, and the source function is a Heaviside step in displacement u_0. The dots indicate the time it takes the strain to reach $[1 - \exp(-1)] = 63$ per cent of the local maximum; the distance divided by this time is the velocity in our model. Dashed lines are plotted for $\eta = 2 \times 10^{18}$ Pa s. (b) Plots of velocity versus distance for different values of viscosity η (units of 10^{18} Pa s).

The observed correlation time of 36 yr and mean distance of 200 km beween the land the sea events translates into an average velocity of 5.6 km yr^{-1}. Using this velocity at a distance of 200 km in our model curves (Fig. 10b) indicates an effective viscosity of about 7×10^{18} Pa s. A 20 per cent uncertainty in both the mean distance and the correlation time translates into a spread in viscosity estimates of $5–12 \times 10^{18}$ Pa s.

Comparison with other studies of viscosity in NE Japan

Heinze and Sacks (1979) studied the post-seismic deformation produced by a large ($M = 7.4$) interplate event in 1973 off the coast of Hokkaido, northern Japan. They fit a viscoelastic model to 4-yr records of horizontal strain, measured by geodetic networks at distances of 50 and 120 km from the source. Their model is identical to ours except for their source function which consisted of two terms; a displacement term u_0 from the sea earthquake and a steady linear reloading term which comes from the compression of the subducting slab. To estimate the reloading term, Heinze & Sacks used a constant rate of subduction inferred from the long-term average recurrence time of 30 ± 15 years for large thrust events throughout Japan during the past 400 yr. (This recurrence time is approximately the reciprocal of the Poissonian rate for the sea events in window A.) Using $H_e = 40$ km, $\mu = 100$ GPa and 2 m of slip in the model, they estimated viscosity in the range ~$1–4 \times 10^{18}$ Pa s and a pulsed stress-drop of the order 0.5–1 MPa (5–10 bars). The stress-drop behaves similar to the velocity, in that it depends on both distance and viscosity. But it also depends on the amount of slip at the source, i.e. the magnitude of the earthquake. In the above instance, it represents a significant percentage of the elastic stress-drops observed in the sea events, which are estimated, for this region of NE Japan, to be in the range 10–100 MPa (0.1–1 kbar) with a mean towards the lower end of the range.

Heinze & Sacks also used the viscoelastic model to study the migration of microearthquake swarms reported by Tanaka (1978) in Tohoku, NE Japan. By assuming that the swarm migrations followed the peak of the strain pulse, and although the swarm data had a large amount of scatter, they inferred a mean pulse velocity of about 25 km yr^{-1}. Use of this velocity in their model curves yielded an estimate of asthenospheric viscosity of 2×10^{18} Pa s, in good agreement with the viscosity estimate from the geodetic strain data.

We believe that the viscosity estimates by Heinze & Sacks are biased towards lower values by their use of a 30 yr reloading time. The estimate of 30 yr is close to the Poissonian rate in window A for the sea events, but the sea events collectively span ~550 km of coastline. In short sections of the Japan Trench (~100 km, i.e. appropriate for the largest thrust events in this region) the recurrence time is in the neighbourhood of 150 yr, in the Poissonian sense. Thus a longer time in the reloading term would be more realistic when modelling subduction in this region of Japan. Viscosity will tend to be underestimated in the model when the reloading term accumulates stress too quickly (i.e. 30 instead of 150 yr), because the net effect of the compression from the reloading term is to counteract and slow down the rarefaction from the strain pulse. The effectiveness of the strain pulse is then diminished and is attributed to (incorrect) reloading rather than to increased viscosity. This may explain to some degree the discrepancy between their viscosity estimates and those in this study. The reloading term will be discussed in more detail in a later section.

A viscoelastic model was also used by Thatcher *et al.* (1980) to analyse uplift data measured five times since 1900 in NE Japan. They found that a very localized depression of about 75 km width, centred close to the fault of the 1896 Riku-U earthquake, has subsided at a continually decreasing rate. This was attributed to viscous relaxation of the asthenosphere from the lithospheric load imposed from the stress-drop of the large Riku-U shock. They fitted the uplift data using a model of an elastic plate over a Maxwell half-space and were able to estimate an effective lithospheric thickness of 30 km and an asthenospheric viscosity of 10×10^{18} Pa s.

Triggering mechanism for the land–sea correlation

In Appendix B, an equilibrium equation for a locked thrust fault is derived from a consideration of the principal forces acting on the fault. At the times in the subduction cycle when there is a high probability for land activity, the thrust zone is also approaching the high stress regime near the peak of the cycle and is primed for failure (see Fig. 7). Under these conditions, the strain pulse may trigger earthquakes in the subduction zone (Appendix B). A large inland earthquake from a high stress zone of the buckled plate will create a stress pulse which diffuses outward at a rate governed by the plate thickness and asthenospheric viscosity. As the pulse sweeps past the thrust fault several decades later, it unloads the fault by producing a net pull of the continental plate away from the subducting slab (see Appendix B). This reduces the static frictional force from the overburden pressure and triggers an earthquake (Fig. 7b). In some sense, the land quakes lower the failure threshold of sea quakes, but only through a relative change of the components of stress acting on the thrust fault; the physical properties of rocks are unaffected.

Triggering is unidirectional. In our model, sea quakes will not trigger land quakes since both normal and shear stress are relieved by the decompression following a large sea event. A trigger pulse can explain the peak in the correlation function since the stress-drop in the thrust zone from the strain pulse varies on a much shorter time-scale than the buildup of background stress from tectonic compression. The lack of periodicity in the recurrence times of the sea quakes in NE Japan is also explained by a trigger; the quasi-cyclic behavior of the sea quakes in the elastic model (Fig. 7a) is interrupted by land quakes following a broad-band (Poissonian) distribution in time. If the strain pulse fails to trigger a sea quake, earthquakes will eventually occur in the manner of Fig. 7(a). The catalogue, however, indicates that this region of the Japan Trench is void of large earthquakes ($M \geq 8$) in contrast to numerous historic great earthquakes in the Nankai Trough of SW Japan. Although a large part of the Nankai Trough looks similar to the Japan Trench, the subducting Philippine sea plate that forms the trough is much younger, and mechanically different, than the older Pacific sea plate. The Philippine plate, estimated to be 20 Myr old in east Japan and 40 Myr old in west Japan, is probably buoyant and more flexible (Ichikawa 1980; Hirahara 1981; Sacks 1983). Being more buoyant, it is less prone to buckle the adjacent land plate and being more flexible, it is less prone to produce earthquakes because of relatively small localized strain changes (see explanation in Appendix B). If the sea events in the Nankai Trough followed the model in Fig. 7(a), more stored strain energy would be released (i.e. larger M) compared to the triggered sea events in Fig. 7(b); this is consistent with the catalogue for this region.

SURFACE DEFORMATIONS AND GEODETIC SURVEY DATA

As the strain pulse diffuses outward from the earthquake source it will deform the land. With a traveltime in the neighbourhood of 40 yr, any instrument-based measurements that may have detected the transit of a strain pulse from land to sea would certainly be fortuitous. In the modern era, the dominant land–sea correlation is from the sea events in 1930–1950 which could have been triggered by the land events in 1895–1915. The epicentres of all these events are plotted in Fig. 11(b). The largest land event ($M = 7.5$) was in Riku-U in 1896; in fact, this produced the largest on-land reverse faulting in Japan of all events in historical times (Matsuda *et al.* 1980).

Geodetic surveys throughout Japan have been conducted by the (then) Military Land Survey Department several times in the modern era since the initial survey in 1884. Specific to the area covering the land events in Fig. 11(b), there were triangulation surveys conducted in 1904 and 1964 (Harada 1967), and levelling surveys in 1898, 1930 and 1950 (Hayashi 1969); triangulation and level surveys measure net horizontal and vertical ground displacements, respectively. Surveys that span the time interval between earthquakes (i.e. after the first and up to, but not including, the second)

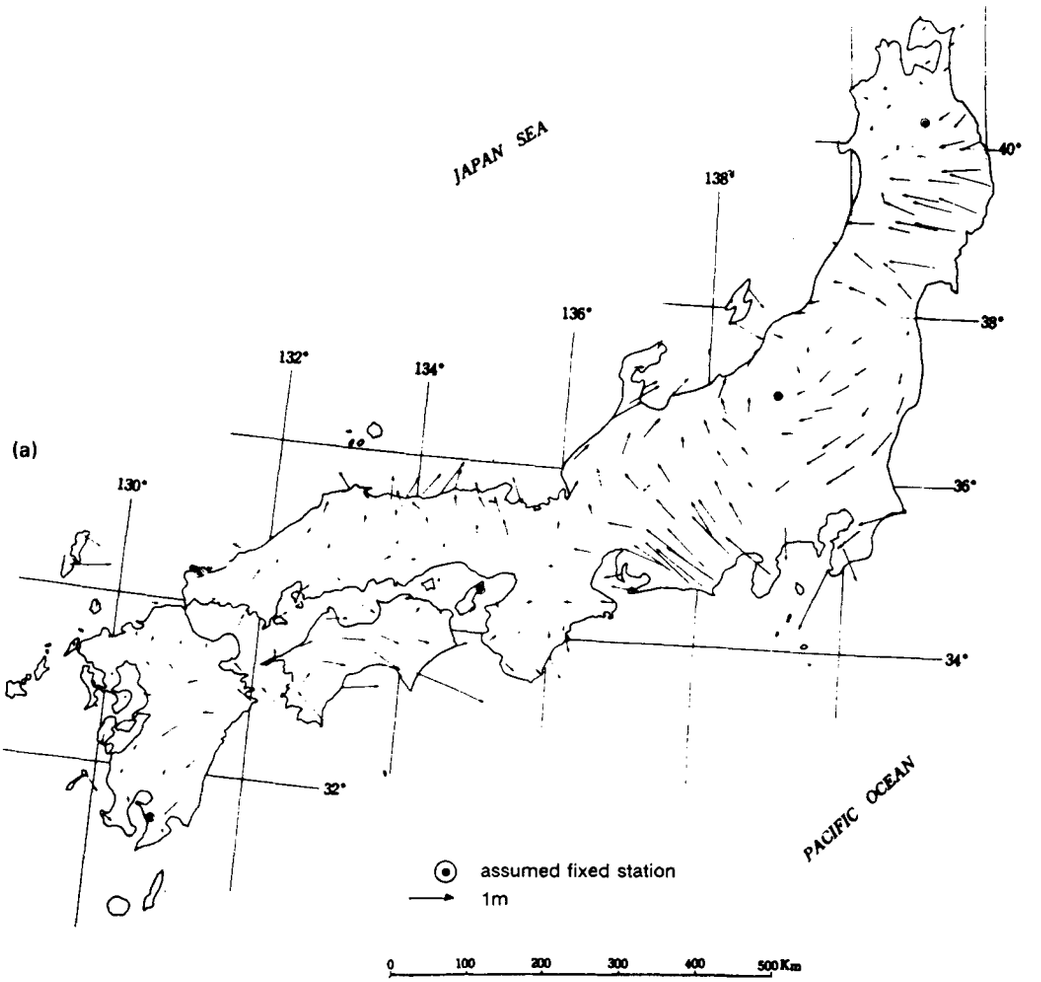

Horizontal Displacements During Half a Century.

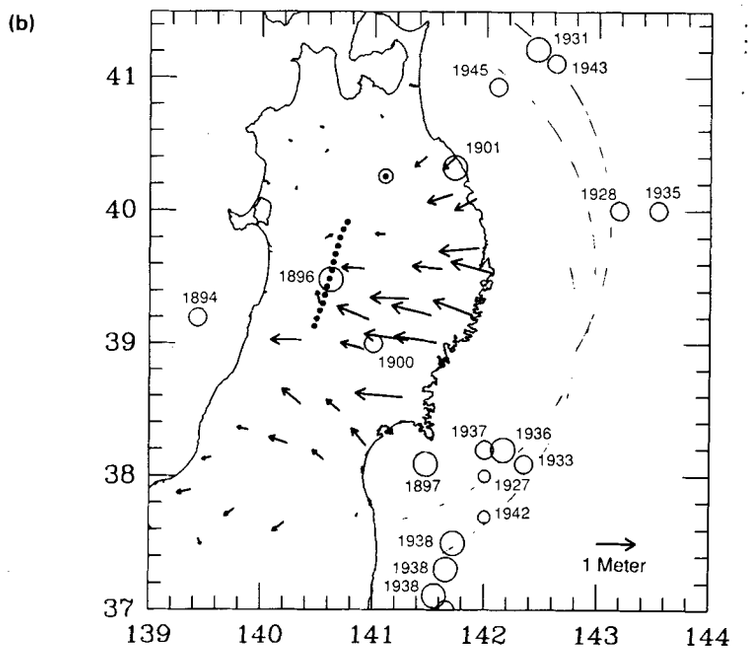

Figure 11. (a) Plot of the horizontal ground displacements (solid arrows) measured from geodetic triangulation surveys in Japan conducted during 1882–1911 and 1948–1967 (from Harada & Isawa 1969). (b) An enlargement of Tohoku, NE Japan. Triangulation surveys were conducted in this region in 1904 and 1964. Also plotted are the major earthquakes in 1895–1915 (land) and in 1930–1950 (sea). The fault line of the large 1896 Riku-U event, determined in part from recent trenching work, is drawn as a thick dotted line. The survey benchmark in this region is located near the northern tip of the fault. The dashed arcs are drawn using a radius of 200 km from the top, middle, and bottom of the Riku-U fault. This radius is the mean distance between the land–sea events in window A (see Table 2) and is consistent with the events drawn here from window B.

are ideally located in time because the large coseismic deformations accompanying each event are excluded. We can therefore search for evidence of post-seismic deformations from a strain pulse. We are fortunate because the triangulation and level surveys in NE Japan commenced several years after the 1896 Riku-U event, but only the first level survey (1898–1930) is entirely between the times of the land and sea events plotted in Fig. 11(b). The next level survey (1930–1950) and the triangulation survey (1904–1964) both include large sea shocks. Nevertheless, inspection of the net vertical displacements from 1890 to 1930 (Fig. 12a) suggests that most, if not all, of the uplift in this region seems to come from the 1896 Riku-U shock. The same conclusion was reached by Thatcher *et al.* (1980). In the next survey, 1930–1950, the uplift in this region appears to be in the noise level of the measurements (Fig. 12b).

It is thus reasonable to assume that the horizontal displacement (Fig. 11) was produced chiefly by the 1896 event. The geodetic survey data is reckoned from an assumed stationary benchmark located about 40 km from the northern tip of the Riku-U earthquake fault (Fig. 11b). We believed that the benchmark was close enough to the fault that no adjustments to the survey data were necessary. This seems justified because in the immediate vicinity of the fault the displacements are only about 10 per cent of the maximum in the figure and have no preferred direction.

In Appendix A solutions are found for the horizontal displacements produced by a thrust event in a model of an elastic plate (lithosphere) overlying a viscous channel (asthenosphere). Using the horizontal survey data in the model, both asthenospheric viscosity and fault slip are estimated.

Viscoelastic model results

Because the solution for the displacement is in integral form (equation A16), it was not possible to fit the horizontal survey data by an inverse least-squares method. Instead, the forward problem was solved and the parameters in our model estimated by minimizing the value of the χ^2 statistic in a grid search. The value of the plate thickness was fixed at 30 km and the elastic modulus at 100 GPa, and then a two-parameter grid was searched for the best fitting values of the fault slip u and the viscosity η in the model. It is assumed that the Riku-U event initiated the diffusive strain field in 1896 from a thrust source of unknown slip u_0. Then using the above fixed (H_e, μ) and variable (u, η) parameters in (A16), absolute horizontal displacements are computed at the survey positions using the elapsed times of 8 and 68 yr (i.e. time intervals from 1896 to the triangulation surveys in 1904 and 1964). The differences between these two calculations are the net displacements or model predictions. The sum of the squared differences between the model predictions and the observed displacements is the χ^2 statistic which is minimized by a gradient-search method of the parameter grid (see Bevington 1969).

The results of the grid search are shown in Fig. 13(a) where contours and the minimum value of χ^2 are plotted; the minimum χ^2 indicates the least-squares estimates of the parameters ($u_0 = 2.6$ m, $\eta_0 = 13 \times 10^{18}$ Pa s). The 95 per cent confidence level in the figure, from which parameter estimates can be inferred, is obtained by a standard calculation using the F-statistic and the minimum χ^2 (see e.g. Jenkins & Watts 1968). The observed data and the best-fitting curve using the least-squares estimates are shown

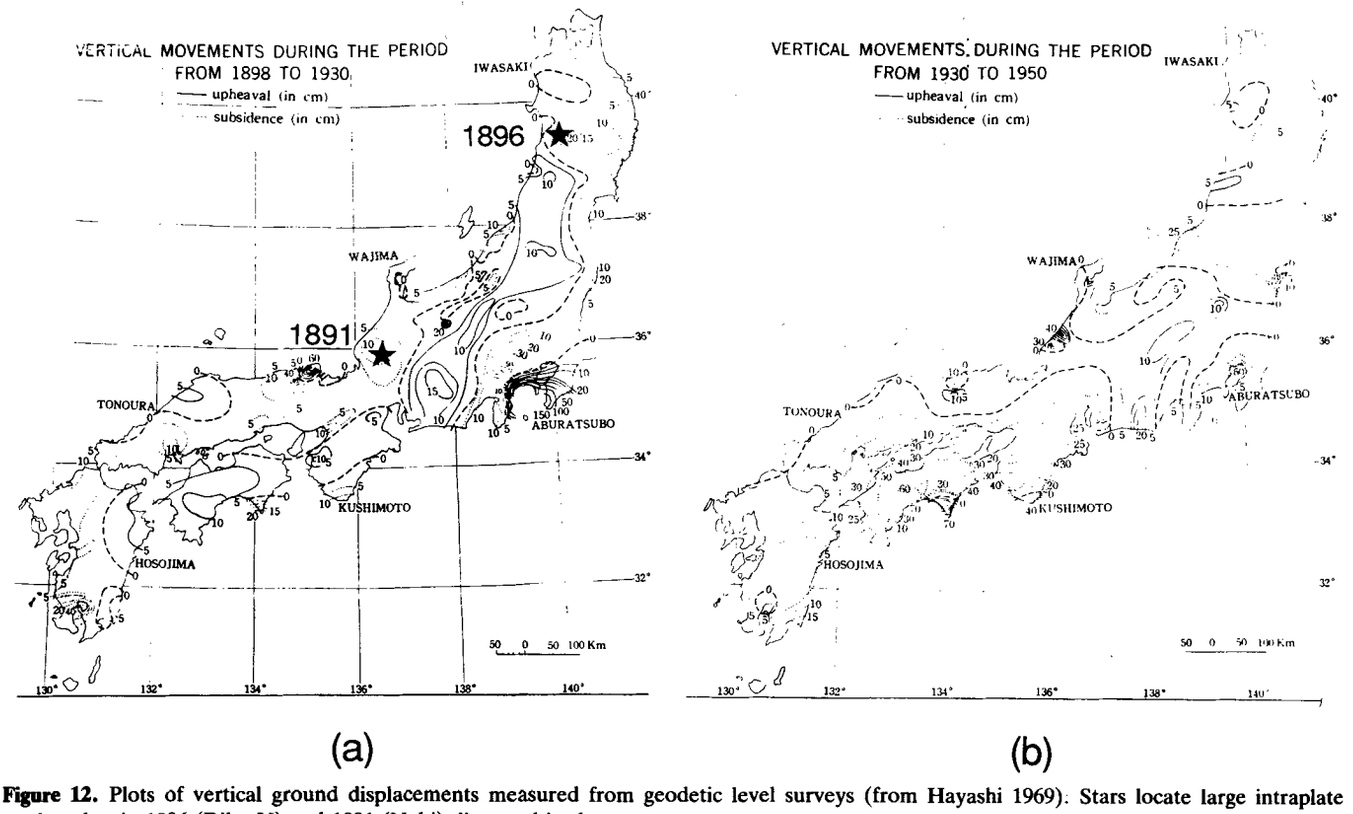

Figure 12. Plots of vertical ground displacements measured from geodetic level surveys (from Hayashi 1969). Stars locate large intraplate earthquakes in 1896 (Riku-U) and 1891 (Nobi) discussed in the text.

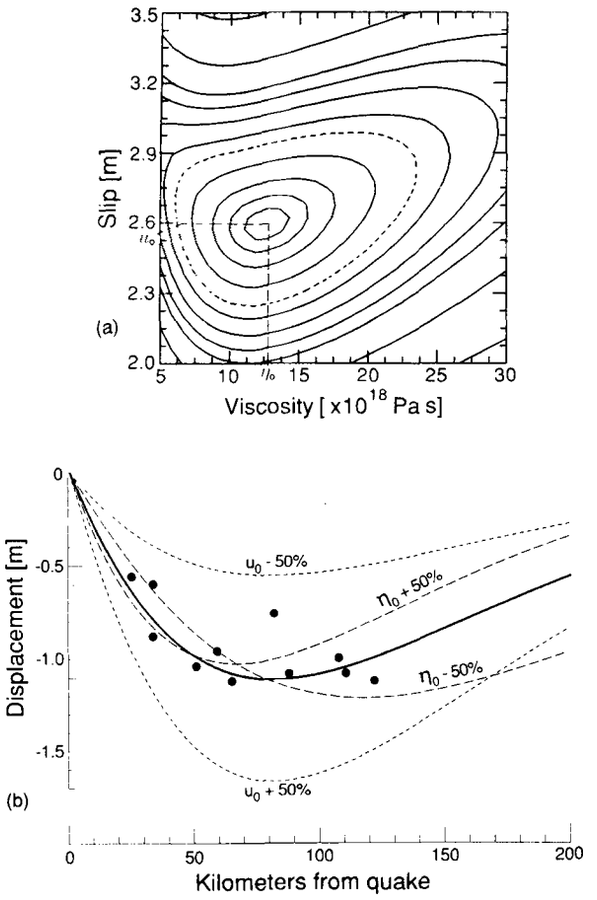

Figure 13. (a) Contours of the χ^2 statistic in the grid search for the least-squares estimates of fault slip u and asthenospheric viscosity η. Minimum χ^2 is located at $u_0 = 2.6$ m and $\eta_0 = 13 \times 10^{18}$ Pa s; dashed contour is drawn at the 95 per cent confidence level. (b) Plot of the relevant horizontal displacements (dots) from Fig. 11 and the model predictions (solid line) using u_0 and η_0. Short-dash lines are drawn for ±50 per cent change in u_0 with η_0 fixed; long-dash lines for ±50 per cent change in η_0 with u_0 fixed.

in Fig. 13(b), along with curves drawn using ±50 per cent variations in the least-squares values. It is found that the viscosity in the model determines the shape and turning point of the displacement curve, whereas the fault slip just scales the displacements. The pulse-like appearance of the curve is an important feature for a good fit to the data which in this case is evident both from the least-squares fit to the data and the roundness and steepness of the contours surrounding the minimum value of χ^2. The viscosity estimate of 13×10^{18} Pa s agrees well with our previous estimate of 7×10^{18} Pa s determined from the land–sea correlation results.

As u_0 estimates the slip of the Riku-U event, this provides a test of the validity of the assumptions made and the theory used. The average displacement determined from surface measurements at seven points over 70 km of the fault was 2 m. However, recent trenching across the fault trace revealed horizontal displacements of 3.2 and 2.3–2.6 m along sections of the fault (Matsuda *et al.* 1980). This shows good agreement with our estimate of 2.6 m.

Reloading from tectonic compression

It was mentioned in the section on previous studies that the compression from the subducting slab in NE Japan acts as a linear reloading term in the viscoelastic model with a time constant in the neighbourhood of 150 yr. To determine how much effect this type of source has on the displacement field in the model, equation (A16) may be solved for a source function which linearly accumulates 3 m of displacement in the thrust zone in 150 yr. The value of 3 m is obtained from the average motion of the Pacific Plate in NE Japan of 0.09 m yr^{-1} (Minster *et al.* 1974) multiplied by 150 yr, and multiplied by Kanamori's (1977) seismic efficiency estimate of 25 per cent for this region. We use our least-squares estimate of viscosity of 13×10^{18} Pa s along with $H_e = 30$ km and $\mu = 100$ GPa in the model. Using the elapsed time of the land–sea correlation (36 yr), the total displacement was computed at two points inland: the first is a point 200 km inland from the thrust zone which corresponds to the position of the benchmark near the Riku-U earthquake, and the second is a point 100 km to the east of the first point which corresponds approximately to the position of the surveys near the coast. The difference between these two displacements is the net amount of movement relative to the assumed stationary benchmark caused by the reloading term in the model. The net movement was 0.15 m in 36 yr, which represents 15 per cent of the total movement of 1 m near the coast from the survey measurements (Fig. 11b). Because of the quality of the deformation data, we believe it is reasonably justified to neglect the reloading term in our analysis.

We end with an interesting observation in Fig. 11(a). A group of large horizontal displacements occurs just west of the Izu Peninsula in SE Japan (~35°N, 138°W). We believe that these are manifestations of the strain pulse from the great Nobi earthquake in 1891, the largest reported inland shock in the entire catalogue. The inability to trigger earthquakes in this region is discussed in Appendix B.

CONCLUDING REMARKS

It has been shown that the intraplate (land) events and the interplate (sea, thrust zone only) events are both temporally and spatially correlated; land quakes lead the sea quakes by about 36 yr with a mean correlation distance of ~200 km. The correlation is consistent with a viscoelastic model (Appendix A) and a triggering model (Appendix B) having the following features.

(1) Both types of earthquakes are due to the same overall tectonic force system in the subduction process.

(2) Because the stress has to be transmitted through the thrust zone, large thrust events unload the adjacent land plate. Therefore, the highest stresses in the land plate are most likely reached before a thrust event.

(3) The deformation of the land plate due to long term applications of subduction stresses causes internal concentrations of stress which results in preferential locations for earthquakes on land.

(4) Because of viscoelastic effects which couple the lithosphere to the asthenosphere, the stress relaxations resulting from large land earthquakes propagate to the locked thrust zone as strain pulses. The mean correlation

distance divided by the mean correlation time gives a pulse speed or strain migration rate which can be used in the viscoelastic model to estimate the viscosity. The pulse acts to pull the continental plate away from the subducting sea plate, thus reducing the frictional term $\mu\sigma_{xx}$ and hence the resistance to shear σ_{xy} which then triggers the release of the accumulated tectonic strain.

(5) The surface deformations resulting from the migration of the strain pulse seem to have been detected in land surveys of Japan. These observations provide an independent estimate of the viscous parameter in the model which is found to be moderately constrained and in reasonable agreement with the viscosity estimated from the land–sea correlation.

ACKNOWLEDGMENTS

We were helped by informative discussions with A. Linde and P. Scott, A. Hasegawa (Tohoku University, Japan), L. Knopoff and Y. Kagan (University of California, Los Angeles), and J. Arthur Snoke (Virginia Polytechnic). We are grateful to D. Forsyth for a critical review of the triggering model. Also thanks to W. Zürn (University of Karlsruhe, Germany) for critical comments. A. Mayi-Sawyer digitized the JMA map.

REFERENCES

Ahrens, T. J. & Schubert, J., 1975. Gabbro-eclogite reaction rate and its geophysical significance, *Rev. Geophys. Space Phys.*, **13,** 383–440.

Awata, Y. & Kakimi, T., 1985. Quaternary tectonics and damaging earthquakes in northeast Honshu, Japan, *Earthq. Predict. Res.*, **3,** 231–251.

Bevington, P. R., 1969. *Data Reduction and Error Analysis for the Physical Sciences,* McGraw-Hill, New York.

Byerlee, J. D., 1977. Friction of rocks, in *Experimental Studies of Rock Data with Applications to Earthquake Prediction,* pp. 55–57, ed. Evernden, J. F., U.S. Geological Survey, Menlo Park, Calif.

Cohen, S. C., 1980a. Postseismic viscoelastic surface deformation and stress: 1. Theoretical considerations, displacement and strain calculations, *J. geophys. Res.*, **85,** 3131–3150.

Cohen, S. C., 1980b. Postseismic viscoelastic surface deformation and stress: 2. Stress theory and computation; dependence of displacement, strain, and stress on fault parameters, *J. geophys. Res.*, **85,** 3151–3158.

Cox, D. R. & Lewis, P. A. W., 1966. *The Statistical Analysis of Series of Events,* Barnes & Noble, New York.

Crump, K. S., 1976. Numerical inversion of Laplace transforms using a Fourier series approximation, *J. Assoc. Computing Machinery,* **23,** 89–96.

Diaconis, P. & Efron, B., 1983. Computer-intensive methods in statistics, *Sci. Am.*, **248, (5),** 116–130.

Elsasser, W. M., 1969. Convection and stress propagation in the upper mantle, in *The Application of Modern Physics to the Earth and Planetary Interiors,* pp. 223–246, ed. Runcorn, S. K., John Wiley, New York.

French, A. S. & Holden, A. V., 1971. Alias-free sampling of Neuronal spike trains, *Kybernetik,* **8,** 165–171.

Harada, T., 1967. Precise adjustment of old and new first order triangulation, and the result in relation with destructive earthquakes in Japan, *Bull. Japan geog. Surv. Inst.*, **7,** parts 3–4, 5–64.

Harada, T. & Isawa, N., 1969. Horizontal deformation of the crust in Japan, *J. Geod. Soc. Japan,* **14,** 101–105.

Hayashi, T., 1969. A study of the vertical movements of the earth's crust by means of the precise leveling, *Bull. Japan geog. Surv. Inst.*, **15,** part 1, 1–67.

Heinze, W. D. & Sacks, I. S., 1979. Toward a quantitative model of stress diffusion after large subduction zone earthquakes: applications to Northern Japan, in *Carnegie Institution of Washington, Yearbook,* pp. 288–298.

Hirahara, K., 1981. Three-dimensional seismic structure beneath southwest Japan: The subducting Philippine Sea plate, *Tectonophysics,* **79,** 1–44.

Ichikawa, K., 1980. Median Tectonic Line of Southwest Japan, *Geol. Soc. Japan,* **18,** 134–142.

Ito, K. & Kennedy, G. C., 1971. An experimental study of the basalt–garnet granulite–eclogite transition, in *The Structure and Physical Properties of the Earth's Crust, Geophys. Monogr. Ser., 14,* ed. Heacock, J. G., AGU, Washington, DC.

Jenkins, G. M. & Watts, D. G., 1968. *Spectral Analysis and Its Applications,* p. 138, Holden–Day, San Francisco, California.

Kagan, Y. & Knopoff, L., 1976. Statistical search for non-random features of the seismicity of strong earthquakes, *Phys. Earth planet. Int.*, **14,** 97–108.

Kanamori, H., 1977. Seismic and aseismic slip along subduction zones and their tectonic implications, in *Island Arcs, Deep Sea Trenches and Back-Arc Basins,* pp. 163–174, eds M. Talwani and W. C. Pitman III, AGU, Washington, D.C.

Matsuda, Y., Yamazaki, H., Nakata, T., & Imaizumi, T., 1980. The surface faults associated with the Riku-u earthquake of 1896, (In Japanese), *Bull. Earthq. Res. Inst. Tokyo Univ.*, **55,** 795–855.

Matsu'ura, M., Tanimoto, T., & Iwasaki, T., 1981. Quasi-static displacements due to faulting in a layered half-space with an intervenient viscoelastic layer, *J. Phys. Earth,* **29,** 23–54.

Melosh, H. J., 1976. Nonlinear stress propagation in the earth's upper mantle, *J. geophys. Res.*, **81,** 5621–5632.

Minster, J. B., Jordan, T. H., Molnar, P. & Haines, E., 1974. Numerical modelling of instantaneous plate tectonics, *Geophys. J. R. astr. Soc.*, **36,** 541–576.

Nur, A. & Mavko, G., 1974. Postseismic viscoelastic rebound, *Science,* **183,** 204–206.

Reasenberg, P., 1985. Second-order moment of central California seismicity, 1969–1982, *J. geophys. Res.*, **90,** 5479–5495.

Research Group for Explosion Seismology, 1977. Regionality of upper mantle around northeast Japan as derived from explosion seismic observations and its seismological implications, *Tectonophysics,* **37,** 117–130.

Rikitake, T., 1976. Recurrence of great earthquakes at subduction zones, *Tectonophysics,* **35,** 335–362.

Rikitake, T., 1982. *Earthquake Forecasting and Warning,* Center for Academic Publications Japan, Tokyo.

Rosenman, M. & Singh, S. J., 1973a. Quasi-static strains and tilts due to faulting in a viscoelastic half-space, *Bull. seism. Soc. Am.*, **63,** 1737–1752.

Rosenman, M. & Singh, S. J., 1973b. Stress relaxation in a semi-infinite viscoelastic earth model, *Bull. seism. Soc. Am.*, **63,** 2145–2154.

Rundle, J. B., & Jackson, D. D., 1977. A three-dimensional viscoelastic model of a strike–slip fault, *Geophys. J. R. astr. Soc.*, **49,** 575–591.

Rundle, J. B., 1978. Viscoelastic crustal deformation by finite quasi-static sources, *J. Geophys. Res.*, **83,** 5937–5945.

Rundle, J. B., 1982. Viscoelastic-gravitational deformation by a rectangular thrust fault in a layered earth, *J. geophys. Res.*, **87,** 7787–7796.

Sacks, I. S., Linde, A. T., Rodriquez, B. A. & Snoke, J. A., 1978. Shallow seismicity in subduction zones, *Geophys. Res. Lett.*, **5,** 901–903.

Sacks, I. S., 1983. The subduction of young lithosphere, *J. geophys. Res.*, **88,** 3355–3366.

Savage, J. C., & Prescott, W. H., 1978. Comment on 'Nonlinear stress propagation in the earth's upper mantle' by H. J. Melosh, *J. geophys. Res.*, **83,** 5005–5007.

Savage, J. C., 1983. A dislocation model of strain accumulation and release at a subduction zone, *J. geophys. Res.*, **88,** 4984–4996.

Seno, T., 1979. Intraplate seismicity in Tohoku and Hokkaido and large interplate earthquakes: A possibility of a large interplate earthquake off the southern Sanriku coast, northern Japan, *J. Phys. Earth*, **27,** 21–51.

Shimazaki, K., 1974. Nemuro-oki earthquake of June 17, 1973: a lithospheric rebound at the upper half of the interface, *Phys. Earth planet. Int.*, **9,** 314–327.

Shimazaki, K., 1978. Correlation between intraplate seismicity and interplate earthquakes in Tohoku, northeast Japan, *Bull. seism. Soc. Am.*, **68,** 181–192.

Tanaka, K., 1978. Propagation characteristics of earthquake and volcanic activity (in Japanese), *Programme and Abstracts, no. 1,* **81,** Seismological Society of Japan.

Thatcher, W. & Rundle, J. B., 1979. A model for the earthquake cycle in underthrust zones, *J. geophys. Res.*, **84,** 5540–5556.

Thatcher, W., Matsuda, T., Kato, T., & Rundle, J. B., 1980. Lithospheric loading by the 1896 Riku-u earthquake, northern Japan: Implications for plate flexure and asthenospheric rheology, *J. geophys. Res.*, **85,** 6429–6435.

Thatcher, W. & Rundle, J. B., 1984. A viscoelastic coupling model for the cyclic deformation due to periodically repeated earthquakes at subduction zones, *J. geophys. Res.*, **89,** 7631–7640.

Turcotte, D. L. & Schubert, G., 1982. *Geodynamics Applications of Continuum Physics to Geological Problems,* John Wiley & Sons, New York.

Utsu, T., 1974. Space–time pattern of large earthquakes occurring off the Pacific coast of the Japanese Islands, *J. Phys. Earth*, **22,** 325–342.

Wahr, J. & Wyss, M., 1980. Interpretation of postseismic deformation with a viscoelastic relaxation model, *J. geophys. Res.*, **85,** 6471–6477.

Yoshii, T., 1979. A detailed cross-section of the deep seismic zone beneath northeastern Honshu, Japan, *Tectonics,* **55,** 349–360.

APPENDIX A

The subject of this appendix is the time dependent displacement field produced by a dislocation in a purely elastic material which is coupled to another material having viscoelastic properties. In the case of the Earth, the dislocation is caused by rupture from an earthquake, the elastic plate is the lithosphere and the viscosity comes from the underlying asthenosphere.

Elsasser (1969) was the first to realize the importance of viscous effects in his study of the 'sliding of the tectosphere over the asthenosphere'. Since this time there have been many publications on the topic of the elastic–viscoelastic coupling of lithosphere to asthenosphere but the bulk of the literature is inappropriate for this particular study (i.e. horizontal displacements from a thrust or edge source) since most researchers are concerned with either the vertical component of deformation, or a strike–slip (screw) dislocation (Rosenman & Singh 1973a,b; Nur & Mavko 1974; Rundle & Jackson 1977; Rundle 1978; Thatcher & Rundle 1979; Cohen 1980a,b; Wahr & Wyss 1980; Rundle 1982; Savage 1983; Thatcher & Rundle 1984). Melosh (1976) has solved the problem for horizontal displacements from a thrust source, but Savage & Prescott (1978), and Rundle (1978) believe that his model of an asthenosphere with a purely viscous non-linear rheology is inadequate and that a Maxwell rheology is more appropriate for both the short-term elastic and the long-term deformational processes within the Earth.

The general solution for the vector displacement from an arbitrarily oriented finite dislocation in a stratified elastic half-space with an intervenient Maxwellian viscoelastic layer has been found by Matsu'ura, Tanimoto & Iwasaki (1981). This solution provides an important and powerful tool in the analysis and interpretation of deformational data, but is excessively complicated for our needs considering the simple geometry and limited availability of data in this study.

Instead, following Heinze & Sacks (1979), we solve the problem of horizontal displacements in an elastic lithosphere overlying a viscoelastic channel (Maxwell solid). The discrete and continuous representations of this model, along with the notations used below, are shown in Fig. A1. The inset in Fig. A1 [after Awata & Kakimi (1985)] shows the relationship between the major intraplate earthquakes and the fault-bounded blocks in NE Japan; the thrust events produce upthrown blocks with crustal shortening. Because of this, we neglected the vertical variation of the displacement in the lithosphere and used a source function of constant horizontal displacement. In addition, we considered only a 2-D line source with no z dependence.

The partial differential equation for the displacement in the lithosphere can be derived from a stress balance by equating the total change of the horizontal stress within a lithospheric element to the shear stress it exerts on an asthenospheric element.

$$H_1 \frac{\partial \sigma_{xx}}{\partial x}\bigg|_{H_1} = \sigma_{xy}\bigg|_{H_1}. \tag{A1}$$

The asthenosphere represents a homogeneous, isotropic Maxwell solid; therefore, the constitutive equation of stress to strain is

$$\dot{\epsilon} = \dot{\epsilon}^{\mu} + \dot{\epsilon}^{\eta} = \frac{\dot{\sigma}}{\mu} + \frac{\sigma}{\eta} \tag{A2}$$

where the dot indicates differentiation with respect to time and ϵ^{μ} and ϵ^{η} are strains due to elastic and viscous deformations, respectively. Thus the shear stress in the asthenosphere can be written as

$$\sigma_{xy} = \mu \epsilon^{\mu}_{xy} = \frac{\eta \, \partial \epsilon^{\eta}_{xy}}{\partial t}. \tag{A3}$$

The shear stress produces a time rate of change of permanent displacement in the asthenosphere but is driven by the difference in displacements in the lithosphere and asthenosphere

$$\sigma_{xy} = \frac{\eta}{H_2} \frac{\partial u'}{\partial t} = \mu \frac{u - u'}{H_2}. \tag{A4}$$

In the perfectly elastic lithosphere the constitutive equation of stress to strain is $\sigma_{xx} = Y \epsilon_{xx} = Y \, \partial u / \partial x$, and when substituted along with (A4) into (A1) results in the partial differential equation

$$H_e^2 \frac{\partial^2 u}{\partial x^2} + u' - u = 0 \tag{A5}$$

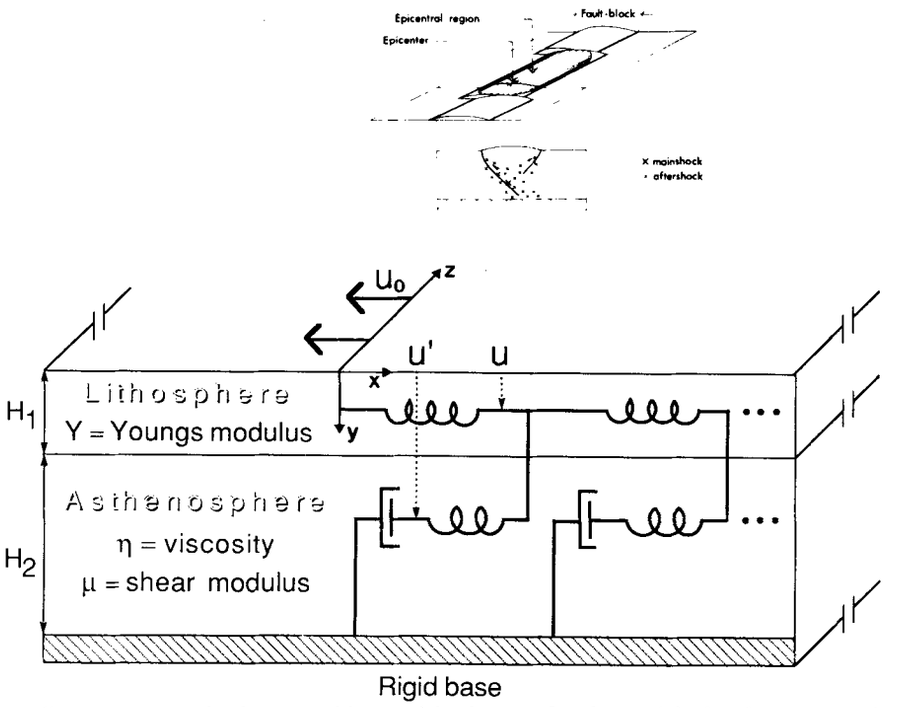

Figure A1. Geometry, coordinate system and other quantities used in the text for the model of a thrust source in an elastic layer over a viscoelastic channel (Maxwell rheology). The network of springs and dashpots is the discrete analogue of the continuous model. The inset shows the relation between the large land events and the fault-bounded blocks referred to in the text.

where the effective elastic thickness is $H_e = \sqrt{(Y/\mu)(H_1 H_2)}$. Both Y and μ are adequately determined from laboratory measurements. Seismic studies [Research Group for Explosion Seismology (1977)] suggest that the elastic thickness of the Japan plate (H_1) is 30 km, in agreement with Thatcher *et al.* (1980). The asthenospheric thickness (H_2) is bounded by the base of the lithosphere and the top of the rigid subducted slab. We have assumed an average thickness of 30 km for H_2 but this estimate could be as large as 45 km. The effect on the viscosity determination is a 10 per cent reduction.

The internal variable u' is the horizontal displacement in the viscous channel and requires another equation for a complete representation of the model. This comes from (A4) where

$$\tau \frac{\partial u'}{\partial t} + u' - u = 0 \tag{A6}$$

in which we have introduced a viscoelastic time constant $\tau = \eta/\mu$. One can eliminate u' from (A5) and (A6) to get the partial differential equation for the horizontal displacement $u(x, t)$ in the lithosphere

$$H_e^2 \frac{\partial^2 u}{\partial x^2} = \tau \frac{\partial u}{\partial t} - \tau H_e^2 \frac{\partial^3 u}{\partial x^2 \partial t}. \tag{A7}$$

The initial conditions in the problem are vanishing displacements and stress for $t < 0$. Hence, equation (A7) is solved by the method of Laplace transforms since then these initial conditions are automatically satisfied. The Laplace transform of (A7) is

$$H_e^2 \frac{d^2 U}{dx^2} = \tau[sU - u(x, 0)] - \tau H_e^2 \frac{d^2}{dx^2}[sU - u(x, 0)] \tag{A8}$$

where $U = U(x, s) = \mathcal{L}[u(x, t)]$ is the Laplace transform with the transform variable s. Another initial condition that $u(x, 0) = 0$ reduces (A8) to the differential equation of simple harmonic motion

$$\frac{d^2 U}{dx^2} = \frac{\tau s}{H_e^2(1 + \tau s)} U \tag{A9}$$

which has the general solution

$$U(x, s) = C_{\pm} \exp\left(\frac{\pm x}{H_e} \sqrt{\frac{\tau s}{1 + \tau s}}\right) \tag{A10}$$

with two arbitrary constants C_+ and C_-. The constant $C_+ = 0$ comes from the boundary value requirement of a finite solution as $x \to \infty$ for all times. The other constant C_- is used to satisfy the boundary value of the source at $x = 0$. The dislocation in Fig. A1 is a fault in the $y - z$ plane with displacement u_0 in the negative x direction; this models an edge dislocation in the lithosphere from a large thrust event. The source function for this type of earthquake is then $u_0 \mathrm{H}(t)$, where $\mathrm{H}(t)$ is the Heaviside step function with Laplace transform u_0/s. (Any source function, such as a possible linear term from tectonic compression, can be easily incorporated into the solution if the Laplace transform is known, which is certainly the case for most elementary functions.) Thus the final form of the transform which solves the partial differential equation subject to the specific initial and boundary conditions is

$$U(x, s) = \frac{u_0}{s} \exp\left(\frac{-x}{H_e} \sqrt{\frac{\tau s}{1 + \tau s}}\right). \tag{A11}$$

As a point of interest we consider two limiting cases of (A11). In the first limit where $\tau s \gg 1$

$$U(x, s) = \frac{u_0}{s} \exp(-x/H_e) \tag{A12}$$

which has the inverse Laplace transform

$$u(x, t) = u_0 \exp(-x/H_e)\mathrm{H}(t) \tag{A13}$$

Since the transform variable s plays the role of 1/(time) and $\tau = \eta/\mu$, we se that (A13) is valid for times much shorter than the viscous time constant. At these times the elastic effects dominate and thus determine the stress field. In the second limit where $\tau s \ll 1$

$$U(x, s) = \frac{u_0}{s} \exp\left(\frac{-x}{H_e}\sqrt{\tau s}\right) \tag{A14}$$

with inverse Laplace transform

$$u(x, t) = 1 - \mathrm{erf}\left(\frac{x}{2H_e}\sqrt{\frac{\tau}{t}}\right) \tag{A15}$$

where erf is the error function. This is a valid solution for times much longer than τ, at which times the viscous effects are responsible for shaping the stress field. Both of the above limiting cases agree with the expected solutions. The general solution

$$u(x, t) = \mathcal{L}^{-1}[U(x, s)] \tag{A16}$$

was obtained numerically using an IMSL subroutine which is based on a method developed by Crump (1976).

The velocity of the strain pulse is computed from (A16) as a function of distance from the source. This is done by first differentiating (A16) with respect to distance to get the strain, $\epsilon(x, t) = \partial u(x, t)/\partial x$. Examples of the strain as a function of time and distance are shown in Fig. 10a. To determine the pulse velocity the standard definition of rise-time in a relaxation process is used which is the time taken (at a given distance from the source) for the strain to rise to $[1 - \exp(-1)] = 63$ per cent of the maximum value; the distance divided by the rise-time is the pulse velocity. (Strain pulses can be positive or negative depending on the sign of u_0 but the characteristic rise-time remains the same.) The rise-time definition plus the fact we are using a 2-D model, means that our velocity is independent of the amount of slip u_0 on the thrust fault, i.e. the magnitude of the earthquake. An alternative way of determining velocity is to find the time (at a given distance) when the strain exceeds some pre-assigned critical value. Using this definition, the pulse velocity will depend on the strength (or earthquake magnitude) of the source and in general these velocities are higher, particularly at shorter distances. In some instances, reported strain velocities are inferred from the migrations of earthquakes and aftershock sequences, which suggests that a critical level of strain has been reached or possibly lowered, as in the framework of our triggering model. Thus in these studies the strength (and shape) of the source is important and cannot be neglected. In fact, a more detailed consideration of both the working definition of velocity, and the strong dependence of velocity on distance, may help to explain the wide range of strain migration rates reported in the literature.

In any case, the pulse velocity is also influenced by the other parameters in the model; H_e, μ, and η. But for our study in NE Japan, we set $H_e = 30$ km, $\mu = 100$ GPa and varied η from $2\text{–}14 \times 10^{18}$ Pa s. The calculated curves of velocity versus distance using the rise-time definition are shown in Fig. 10(b). The observed land–sea correlation of 200 km and 36 yr translates into a velocity of 5.6 km yr^{-1} which in Fig. 10(b) indicates a viscosity estimate of $\sim 7 \times 10^{18}$ Pa s.

APPENDIX B

A schematic diagram of the major forces acting across the interface in a subduction zone is shown in Fig. B1: F_T is from the tectonic compression caused by the movement of the sea plate towards the land plate, F_S is the in-slab force from the downward pull of the sinking portion of the slab (if any), and F_R is the force from the combined effects of overburden pressure and the flexural rigidity of the bent slab. The force F_P is occasional, produced by the passage of a stress pulse from an interplate earthquake.

The fault is assumed stationary between earthquakes, thus modified Coulomb equilibrium holds

$$\sigma_S \leq \mu\sigma_N \tag{B1}$$

where μ is the coefficient of friction and σ_N and σ_S are the normal and shear stress across the fault, respectively. We can write (B1) in terms of the components of the forces as

$$F_S + (F_T - F_P)\cos\theta \leq \mu(F_T - F_P)\sin\theta + \mu F_R \tag{B2}$$

or

$$F_S \leq (F_T - F_P)(\mu\sin\theta - \cos\theta) + \mu F_R. \tag{B3}$$

Ignoring F_P for a moment, the equality in (B3) forms a linear relation between F_S and F_T with slope $\alpha = (\mu\sin\theta - \cos\theta)$ and intercept μF_R. This divides the plot of F_S versus F_T (Fig. B2) into two regions; faults in the upper region continually slip while faults in the lower shaded region are locked, can therefore buildup a shear stress and then fail to produce earthquakes. Most subduction zones are seismically active and therefore in the locked regime.

The force F_R is necessary in (B3) to stabilize the thrust fault against the action of the compressional and sinking forces. In NE Japan, the dip angle of the subducting Pacific

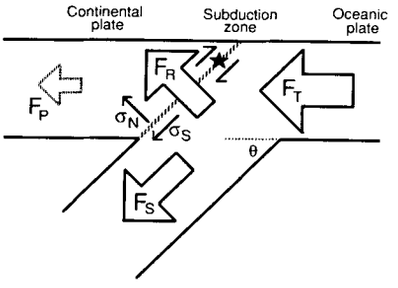

Figure B1. Schematic diagram of the principal forces acting across the thrust fault in a subduction zone: F_T is the tectonic compression from sea floor spreading, F_S is the sinking force, F_R is from the combined effects of overburden pressure and elastic rigidity of the bent slab, and F_P is the occasional force from the stress pulse of an intraplate earthquake. Since F_P is from a rarefaction it has the opposite sign to F_T.

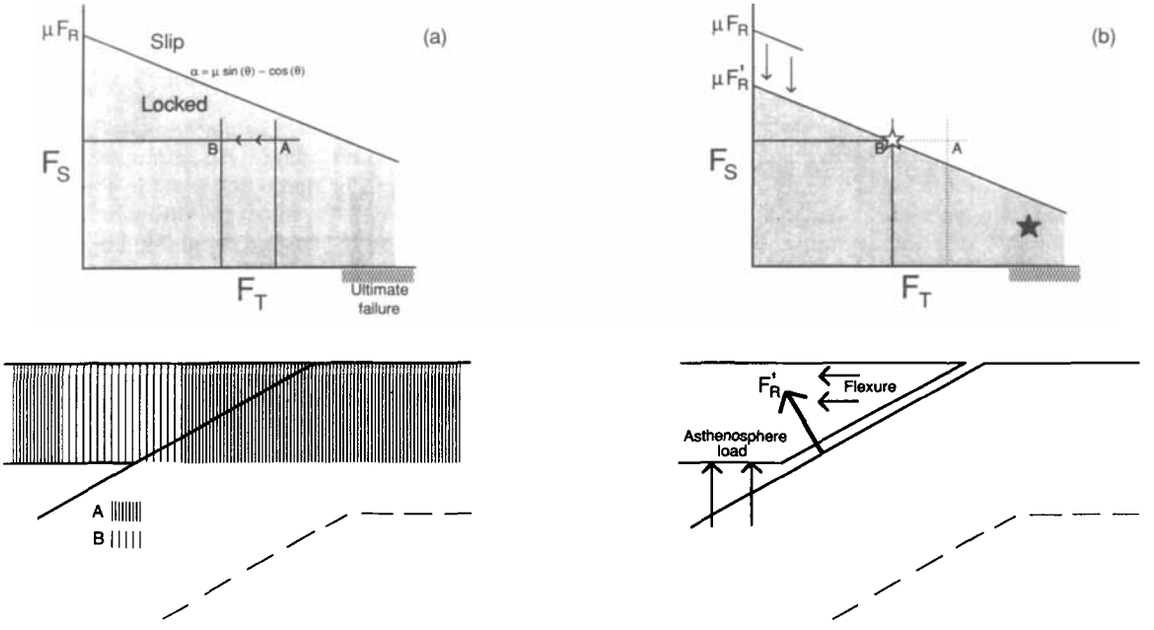

Figure B2. Qualitative plot of F_S versus F_T. The solid line in (a) with negative slope and intercept μF_R is the solution to the equality in (B3) without the term F_P. Faults above the line will slip, while faults in the shaded region below are locked. Inclusion of the force $F_P = \gamma F_T$ from a stress pulse into (B3) will have two effects: (a) Superposition of the tectonic compression and the pulse rarefaction will move points in the locked regime to lower values of $F_T(A \rightarrow B)$, and (b) the straight line is shifted downward because the continental plate tends to pull away from the subducting slab which reduces the overburden pressure and thus the static frictional term μF_R. In the case shown, the overburden pressure on the thrust fault is relieved and redistributed as a load on the asthenosphere (temporarily) and a flexure of the continental plate. The net result of these two effects is the formation of new region in the plot where faults, which were originally locked, will now slip; i.e. the pulse triggers earthquakes. Young subducting slabs having a small sinking force F_S (maybe even buoyant) will lie below the trigger region. Here, a strain pulse is unable to unlock the thrust fault enough to trigger an earthquake, hence an earthquake (solid star) will occur when F_T exceeds the yield strength of the fault. Older and colder slabs that sink would have a larger F_S and may lie within the trigger region. Here, a strain pulse will trigger an earthquake (open star) at a stress buildup F_T below ultimate failure.

plate is determined from seismic studies to be about 30°. Using this value, and a coefficient of static friction $\mu = 0.85$ (see e.g. Byerlee 1977) in (B3), results in a negative slope $\alpha = -0.44$; the slope is negative because the dip angle is below the critical angle $\theta_c = \tan^{-1}(1/\mu) = 49.6°$. Thus without the term μF_R in (B3), an isolated fault under these conditions is unstable and will continually slip when subjected to any compressional force F_T. The overburden pressure and the internal rigidity of the slab lock the fault at the shallow dip angle by generating a static friction force μF_R which is independent of tectonic compression and which overcomes the combined shearing force $F_S + F_T \cos\theta$. Before a thrust event, the combination of forces discussed above is in stable equilibrium in the locked portion of Fig. B2.

Now consider what happens when the force term F_P from the stress pulse is included in (B3). The amplitude of this force is set at some percentage of the tectonic force, $F_P = \gamma F_T$. This assumption is reasonable because a larger tectonic compression will produce a larger magnitude intraplate earthquake, which in turn will generate a larger stress pulse. A rough estimate of γ can be obtained as follows. In this region the Pacific plate converges at a rate of ~ 9 cm yr^{-1} and the recurrence time is ~ 150 yr, thus there is a possible 14 m of 'compression'. Since the thrust zone here has only a 25 per cent seismic efficiency (Kanamori 1977), 3/4 of the motion may not store strain energy or be involved in deformation of the land plate. As a lower limit, we therefore assume that only 3 m of 'compression' actually occurs. The survey data indicates ~ 1 m of deformation from the stress pulse, which suggests that γ could be as large as ~ 30 per cent.

Including the term F_P into the force balance (B3) has two effects. The first effect is to decrease the tectonic compression. Since stress is continuous across the thrust fault, the rarefaction from the stress pulse F_P can be added to the compressional term F_T in accordance with the superposition principle of linear elasticity. As shown in the force plot in Fig. B2(a), this will cause a point in the locked regime to move towards a lower compression by an amount $F_P = \gamma F_T$ along a line of constant F_S (the sinking force is unaffected by the stress pulse). This tends to increase the locking of the fault, since at sub-critical dip angles the stress pulse is more effective in reducing the tectonic shear stress ($F_T \cos\theta$) than the tectonic frictional stress ($\mu F_T \sin\theta$) across the fault.

The second effect is the reduction of the static frictional term μF_R. In NE Japan the oceanic plate is ~ 3 times thicker than the continental plate. Also, once past the thrust zone, the subducting slab is securely anchored to great depths by the surrounding asthenosphere. From the point of view of a stress pulse, the oceanic plate is essentially fixed when compared to the continental plate. This does not imply that the oceanic plate is immovable, simply that it moves in a

manner to minimize pumping of the asthenosphere. As the stress pulse diffuses outward from the inland source the continental lithosphere is horizontally displaced by an amount

$$d(x, t) = \int_{\text{source}}^{x} \frac{\epsilon(x', t)}{\kappa} dx'. \quad \text{(B4)}$$

where $\epsilon(x', t)$ is the strain from the pulse and κ represents the mechanical stiffness of the system. Because the subducting slab taken as a whole is mechanically much stiffer than the continental plate ($\kappa_{\text{ocean}} > \kappa_{\text{land}}$), there will be a differential displacement across the fault which increases with time, i.e. the continent will tend to be pulled away from the subducting slab (Fig. B2b, see also Fig. 11b). When this happens, a portion of the weight of the continental plate that was originally supported by the subducting slab at the thrust zone is now supported both by internal elastic stresses and the asthenosphere (Fig. B2b). As an illustrative example, consider the case where the plates are rigid and the oceanic plate is immovable. The slightest displacement from a stress pulse will pull the continental plate clear of the subducting slab and completely unload the thrust fault ($F_R = 0$). The overburden weight that was loaded on the thrust fault will be redistributed as a load (temporarily) on the asthenosphere (Fig. B2b). And as soon as the weight is removed, the fault is unlocked and ruptures. Of course, oceanic plates are moveable and have finite rigidity, but any amount of differential displacement will affect the static frictional term μF_R by unloading the normal stress to some extent, thus lowering the intercept in (B3) as shown in Fig. B2(b).

The above two effects may perturb the force balance to the extent that certain faults that were initially locked will now slip; i.e. the pulse triggers earthquakes. Therefore earthquakes occurring in the locked zone of Fig. B2 will be of two types: either triggered by stress pulses (open star), or occurring because the ultimate yield strength of the fault is reached (solid star). Real thrust zones are more complicated than our simple qualitative model. Nevertheless, we show below that the simple picture is consistent with the magnitude cut-offs of the largest shocks seen in several subduction zones.

Kanamori (1977) and Sacks (1983) have studied both young and old subducting slabs and found that both the amount of sinking (F_S) and the degree of coupling (F_T and F_R) in thrust zones is highly variable. Generally, dense old slabs sink, and less-dense young slabs may be buoyant but if the basaltic crust of a subducting slab is transformed into eclogite (a very dense phase), ocean floor of any age will sink. The basalt-eclogite transformation is discussed further by Ito & Kennedy (1971), Ahrens & Schubert (1975), and Sacks (1983).

A young buoyant slab will have small F_S and be tightly coupled to the land plate. An example of this is the subduction of the Philippine Sea plate in the SE portion of the Nankai Trough. A study by Hirahara (1981) suggests that here the slab dips down to about 60-km depth and then levels off horizontally. Sacks (1983), using this and other observations, concluded that the slab has a negative F_S (is buoyant) and is coupled against the continental plate over an area much larger than just at the thrust zone. Subduction of this type would be located in the lower right-hand portion of Fig. B2(b) (solid star). Since this region is unaffected by the downward shift in the line from the strain pulse (if any, and at least for practical values of γ) earthquakes here will not be triggered but will occur when the yield strength is reached (see also Fig. 7a). This may explain why this region of the trough produces the largest thrust events ($M \geq 8$) in the historic Japanese catalogue.

An example of an older and therefore colder and denser slab is the subducting Pacific plate (>100 Myr) in the Japan Trench. In the region where we observe the land–sea correlation the slab bends and then sinks with minimal contortion to great depths. This slab and others undergoing normal (sinking) subduction, would tend to be located more towards the middle of Fig. B2(b) (open star). At this location in the plot, a strain pulse would shift the line past the primed thrust zone and trigger an earthquake (see also Fig. 7b). If the strain pulse is too weak to trigger earthquakes, rupture still will occur as in Fig. 7(a). However, the observed land–sea correlation in the earthquake catalogue for the last 400 yr suggests that almost all of the thrust events were triggered (Fig. 3b). This can explain the absence of large earthquakes ($M \geq 8$) in the catalogue for this region.

A final example is the subduction of the Philippine Sea plate in the Kyushu region of the SW Nankai Trough. Although the oceanic plate here is relatively young (~40 Myr), Sacks (1983) inferred from the work of Hirahara (1981), that unlike the buoyant SE portion of the trough, the subduction is normal (i.e. the slab sinks). According to our model, the thrust earthquakes in this region could be triggered. Unfortunately, the historic reports of land seismicity are insufficient to test this hypothesis, but the catalogue shows no large thrust events ($M > 8$) in the Kyushu region of the trough. All the above observations are consistent with our simple triggering model.